Archaeal community composition in Holocene methane pockmarks of the Gdańsk Basin (Baltic Sea, Poland): insights from tetraether lipids and 16S rRNA analysis

Izabela De Mey-Śnieżyńska[1*], Mirosław Słowakiewicz[1], Francien Peterse[2], Aleksandra Brodecka-Goluch[4], Andrzej Borkowski[3], Katarzyna Łukawska-Matuszewska[4]

[1]University of Warsaw, Faculty of Geology, 02-089 Warsaw, Poland

[2]Utrecht University, Department of Earth Sciences, 3584 CS Utrecht, The Netherlands

[3]AGH University of Krakow, Faculty of Geology, Geophysics and Environmental Protection, 30-059 Kraków, Poland

[4]University of Gdańsk, Faculty of Oceanography and Geography, 81-379 Gdynia, Poland

*Corresponding author: i.sniezynska@uw.edu.pl

Highlights

Pockmark sediments harbour substantially higher archaeal diversity and abundance compared with non-pockmark reference sediments.

Pockmarks appear to function as tightly coupled metabolic systems, in which various archaeal groups potentially cooperate in methanogenesis, whereas non-pockmark sites contain less integrated, loosely coupled sub-communities.

The MET4 pockmark in the Gdańsk Deep hosts the most diverse and abundant methanogen community, coinciding with the highest concentrations of isoprenoid glycerol dialkyl glycerol tetraether lipids (iGDGTs). However, iGDGT indices indicate mixed archaeal sources rather than methanogenic lipid sources.

Crenarchaeol dominates the iGDGT in both pockmark and reference sediment cores, suggesting strong AOA-related iGDGT synthesis. However, Nitrososphaeria-related sequences are not dominant in the sedimentary archaeal community, indicating a pelagic origin of crenarchaeol.

Abstract

Methane pockmarks and shallow gas systems are prominent geomorphological features in the Baltic Sea that act as hotspots of microbial activity. In the Gdańsk Basin, pockmarks vary in gas-seepage intensity and in the extent of freshened porewater discharge, both of which influence the archaeal community structure and the composition of internal methane biofilters. The objective of this study was to examine the effects of methane seepage and freshened porewater on the composition of archaeal communities and on the isoprenoid glycerol dialkyl glycerol tetraethers (iGDGTs), membrane lipids synthesised by these communities, across the gas systems examined. Additionally, the effects of these environmental factors on the use and interpretation of iGDGT-based proxies under conditions of gas and water seepage were assessed. The study investigates whether iGDGT patterns in these Baltic gas systems reflect methane-driven processes, including anaerobic oxidation of methane (AOM) and methanogenesis, porewater freshening, or pelagic contributions from ammonia-oxidising archaea (AOA). The results show elevated iGDGT concentrations in pockmark cores compared with reference non-pockmark cores; however, the iGDGT distribution is site-specific. Overall, iGDGT concentrations are much higher at sites with reduced pockmark activity and weak porewater freshening. Nevertheless, consistently low Methane Index values (MI < 0.09), together with low GDGT-0/crenarchaeol (< 1) and low GDGT-2/cren (< 0.04) ratios, indicate that the iGDGT pool lacks the typical enrichment in GDGT-1 to -3 associated with AOM, suggesting no AOM imprint on the iGDGT pool. However, 16S rRNA analysis revealed that the anaerobic methanotrophic archaeal lineages (ANME) consist of ANME-2b and ANME-3. A strong positive correlation between OH-GDGTs and crenarchaeol, together with the consistency of OH-GDGT% values with those previously reported for Baltic Sea surface sediments, suggests a thaumarchaeal source of iGDGTs in the studied pockmark and reference cores. The Branched and Isoprenoid Tetraether index values suggest marine archaeal GDGT production. In this system, iGDGT-based proxies primarily reflect a strong pelagic presence of AOA, as indicated by the dominance of crenarchaeol. This suggests that, despite the local presence of methanogenic and ANME-related archaeal groups, methane-related AOM does not influence the iGDGT signal due to the archaeal community structure. These findings highlight the complex interplay between freshened porewater and gas seepage in shaping archaeal communities, iGDGT composition, and the sedimentary record. iGDGT-based indices should be used as part of a multi-proxy approach in environmental research.

Keywords: methane, pockmarks, iGDGTs, ammonia-oxidising archaea, crenarchaeol, Holocene, Gdańsk Deep, Baltic Sea

1 Introduction

Pockmarks are concave geological structures ranging from 1 to over 100 m in width and from less than 1 to 100 m in depth, formed by gas and/or water seepage from the sediments into the hydrosphere (King and MacLean, 1970; Hovland and Judd, 1988). As indicators of hydraulic activity, they are categorised as active or inactive depending on whether gas and/or water seepage is continuous or dormant/intermittent (Hovland and Judd, 1988; Hovland et al., 2002). Their seabed depressions facilitate detection through geophysical and hydroacoustic surveys, making them practical proxies for investigating seepage phenomena (Hovland and Judd, 1988). The formation of pockmarks requires pressure buildup in fine-grained, low-permeability sediments, with methane (CH_4) the most commonly emitted component owing to its high mobility (Hovland and Judd, 1988). Seepage types vary globally and include biogenic, thermogenic, or hydrothermal gas seepage; groundwater; or combined gas-and-water seepage (Hovland and Judd, 1988). Pockmarks predominantly form along salt-dome margins (Schmuck and Paull, 1993; Taylor et al., 2000) and in dislocation zones, faults, and bedrock fractures (Shaw et al., 1997). They also occur in regions of low seismicity, such as Sweden (Hovland et al., 2002) and the southern Baltic Sea (Idczak et al., 2020). Glacial and post-glacial processes can influence their formation by generating overpressure, as observed in the North Sea (Callow et al., 2021) and the Baltic Sea (Whiticar and Werner, 1981; Whiticar, 2002; Kreuzburg et al., 2023). Baltic Sea pockmarks have been documented in Eckernförde Bay and the Mecklenburg Bight (Werner, 1978; Wever et al., 1998; Jensen et al., 2002; Schlüter et al., 2004; Hoffmann et al., 2020; Díaz-Mendoza et al., 2023), the Stockholm Archipelago (Jakobsson et al., 2020), offshore Finland (Virtasalo et al., 2019), and the Gdańsk Basin (Pimenov et al., 2010; Majewski and Klusek, 2011; Brodecka et al., 2013; Jaśniewicz et al., 2019; Idczak et al., 2020; Brodecka-Goluch et al., 2022). The Gdańsk Basin is the focus of this study.

In several Baltic settings, pockmarks have been linked to submarine groundwater discharge (SGD), broadly defined as the movement of fresh, brackish, or saline groundwater into the sea or ocean across the sediment-water interface. SGD encompasses both the inflow of freshened groundwater and the recirculation of saline porewater or seawater, driven by hydraulic pressure and density differences (Burnett et al., 2003, 2006; Moore, 2010; Taniguchi et al., 2019). Evidence of an association between pockmarks and upward groundwater infiltration has been documented in areas such as Eckernförde Bay (Bussmann and Suess, 1998; Schlüter et al.,

2004), Hanko Bay (Virtasalo et al., 2019; Purkamo et al., 2022), and the central Gulf of Gdańsk (Szymczycha et al., 2016; Idczak et al., 2020). In shallow and coastal Baltic regions such as the Bay of Puck, SGD is often described as the movement of recirculated seawater and its dissolved constituents (Piekarek-Jankowska, 1996; Szymczycha et al., 2016). Such groundwater-seawater mixing zones are commonly referred to as subterranean estuaries in permeable coastal aquifers (Moore, 1999; Ruiz-González et al., 2021). However, this framework has not been explicitly demonstrated for the deeper, fine-grained methane pockmarks of the central Gulf of Gdańsk, where available evidence instead points to localised porewater freshening, indicated by chloride (Cl^-) and sulphate (SO_4^{2-}) depletion, linked to seepage of freshened groundwater or discharge of freshened porewater (Szymczycha et al., 2018; Idczak et al., 2020; Brodecka-Goluch et al., 2022; Kurowski et al., 2024; Łukawska-Matuszewska and Dwornik, 2025; Łukawska-Matuszewska et al., 2025). The impact of SGD discharge on pockmark sediments depends on the source, chemical composition, and flow regime of the discharging fluids. Nevertheless, freshened SGD and associated porewater transport can alter the distribution of dissolved species, including NH_4^+, CH_4, dissolved inorganic carbon (DIC), H_2S, Cl^-, and SO_4^{2-}, thereby shifting redox transition zones and influencing CH_4 cycling (Schlüter et al., 2004; Liu et al., 2017; Idczak et al., 2020; O'Reilly et al., 2021; Brodecka-Goluch et al., 2022; Zhang et al., 2025). In the Gdańsk Basin, pockmarks, Cl^- and SO_4^{2-} depletion linked to freshened porewater discharge may weaken SO_4^{2-}-driven anaerobic methane oxidation (S-AOM), promote shallow methanogenesis, and contribute to episodic gas release into the water column.

At the sulphate-methane transition zone (SMTZ) in CH_4-rich sediments, SO_4^{2-} and CH_4 meet, enabling anaerobic oxidation of methane (AOM) (Zehnder and Brock, 1980; Boetius et al., 2000), mediated by sulphate-reducing bacteria (SRB) and anaerobic methanotrophic archaea (ANME) (Knittel and Boetius, 2009), which limit methane emissions to the water column (Reeburgh, 2007). In the Baltic Sea, a halocline at 60-80 m separates oxygenated and anoxic waters, structuring key biogeochemical cycles (Kuliński et al., 2022), including an oxic-suboxic nitrogen-cycling zone driven by ammonia-oxidising archaea (AOA) (Berg et al., 2015b; Jäntti et al., 2018). Archaeal biomarkers for methane cycling (ANME, methanogens) and nitrification (AOA), such as intact polar GDGTs (IPL-GDGTs), can be transported and preserved as core isoprenoidal GDGTs (CL-iGDGTs) in sediments (Schouten et al., 2013).

Archaeal iGDGTs are membrane lipids whose structures adapt to environmental changes (De Rosa et al., 1977; Huguet et al., 2006; Liu et al., 2017; Schouten et al., 2002, 2013; Sinninghe

Damsté et al., 2022). In marine sediments, GDGT-0 and crenarchaeol dominate, with crenarchaeol produced by Thaumarchaeota (Sinninghe Damsté et al., 2022) – in current nomenclature, Nitrososphaerota (Rinke et al., 2021), the main ammonia oxidisers (Berg et al., 2015a, b) and iGDGT synthesisers in the Baltic Sea (Labrenz et al., 2010; Wittenborn et al., 2023). Methanogens primarily produce GDGT-0, whereas methanotrophs, mainly ANME-1, produce GDGT-1 to -3 (Koga et al., 1993; Pancost et al., 2001; Weijers et al., 2006; Rossel et al., 2008; Blaga et al., 2009; Zhang et al., 2011; Inglis et al., 2015; Słowakiewicz et al., 2016; Petrick et al., 2019). Hydroxylated-GDGTs (OH-GDGTs) are produced primarily by Thaumarchaeota (Sinninghe Damsté et al., 2002; Liu et al., 2012; Kaiser and Arz, 2016; Elling et al., 2017; Bale et al., 2019; Sinninghe Damsté et al., 2022), but can also be biosynthesised by methanogens or ANME (Liu et al., 2012; Guan et al., 2024; Fenies et al., 2026). OH-GDGT synthesis reflects cold adaptation (Liu et al., 2012) and salinity changes (Sinninghe Damsté et al., 2022); OH-GDGT-0 is most abundant at high latitudes (Huguet et al., 2013; Varma et al., 2024) and in Baltic Sea sediments, where culture studies have confirmed an AOA source (Blainey et al., 2011; Berg et al., 2015a).

Subterranean estuaries provide a useful conceptual framework for SGD-affected systems, because microbial activity in these groundwater-seawater mixing zones can modify the chemical composition of groundwater before it reaches the seabed (Ruiz-González et al., 2021) 2021). In particular, distinct ammonia-oxidising archaea (AOA) populations occupy deeper freshwater-saltwater mixing zones (Santoro et al., 2008; Rogers and Casciotti, 2010; Purkamo et al., 2022; Wilson et al., 2024). These observations are relevant to archaeal lipid studies because, as noted above, iGDGTs are primarily associated with Nitrososphaerota, whereas GDGT-0 may also originate from methanogenic Euryarchaeota. Although direct studies of GDGTs in SGD-affected marine sediments remain scarce, groundwater research indicates that both CL-iGDGTs and intact polar iGDGTs (IPL-iGDGTs) are produced in situ by indigenous subsurface microbial communities, and that their distributions are linked to groundwater thaumarchaeal groups rather than solely to allochthonous surface inputs (Ding et al., 2018). In the Baltic Sea, the synthesis of iGDGTs is strongly influenced by Nitrosopumilus-dominated archaeal communities (Wittenborn et al., 2023). However, OH-GDGT distributions are highly sensitive to salinity changes (Sinninghe Damsté et al., 2022). Therefore, in methane pockmark sediments affected by porewater freshening, archaeal 16S rRNA and CL-iGDGT distributions may reflect overlapping controls: the regional presence of Baltic AOA, CH_4-driven processes including methanogenesis and methanotrophy, and an additional hydrogeochemical imprint

associated with porewater freshening. This makes such pockmarks a useful natural setting for testing whether archaeal lipid signatures primarily reflect pelagic marine production, CH_4 cycling, or the influence of freshened porewater.

2 Materials and methods

2.1 Study area

Pockmarks in the Gdańsk Deep and the central Gulf of Gdańsk (Fig. 1) occur at water depths of 1-100 m and are characterised by active gas seepage from Holocene silts and clays (Idczak et al., 2020). Although the gas is predominantly biogenic (Brodecka-Goluch et al., 2022), the presence of helium (up to 0.39%) (Idczak et al., 2020) and noble gases (Ne, Ar, Kr, Xe) (Brodecka-Goluch et al., 2022) in samples from station MET1 suggests that these pockmarks vent Middle Cambrian reservoirs, with gas migrating through sedimentary layers along faults (Jaworowski et al., 2010; Idczak et al., 2020; Brodecka-Goluch et al., 2022), possibly with additional contributions from the crust and mantle (Kotarba, 2010; Pokorski, 2010; Kotarba and Lewan, 2013; Kotarba and Nagao, 2015).

The study area spans the Gdańsk Basin and includes stations MET3 and MET4 in the northern Gdańsk Deep, and MET1-MP and MET1-BH in the Gulf of Gdańsk (Fig. 1). The southern stations (MET1 area) receive a high input of terrestrial organic matter from the Vistula River, trap plant material and organic debris, and experience moderate anthropogenic contamination, resulting in elevated TOC (Idczak et al., 2020; Brodecka-Goluch et al., 2022; Łukawska-Matuszewska et al., 2022; Szymczak-Żyła and Lubecki, 2022). Sedimentation rates are lower in MET3 and MET4 (~0.17–0.20 cm yr^{-1}) than at MET1 (~0.15–0.22 cm yr^{-1}) (Szczepańska and Uścinowicz, 1994; Brodecka-Goluch et al., 2022). In a previous study of pockmarks in the Gdańsk Deep, Brodecka-Goluch et al. (2022) reported that methane at pockmark MET3 has isotopic signatures of marine microbial gas, whereas gas venting from MET1-MP shows mixed marine and terrestrial signatures, indicating the upward infiltration of freshwater. Thus, methanogenic pathways vary between sites: acetoclastic at MET1-BH, hydrogenotrophic at MET3, and mixed at MET1-MP (Idczak et al., 2020; Brodecka-Goluch et al., 2022). The MET1 pockmarks are characterised by intensive/periodic gas and freshwater seepage (Idczak et al., 2020; Brodecka-Goluch et al., 2022). MET4 represents the least-studied system, located within a field of multiple pockmarks (Brodecka-Goluch et al., 2020).

In the Gdańsk Basin, SGD is divided into shallow/coastal and deep/offshore components. The shallow/coastal component occurs in nearshore areas and is fed by Quaternary-Cretaceous coastal aquifers (e.g., Piekarek-Jankowska, 1996; Szymczycha et al., 2016, 2018). By contrast, the deep/offshore component comprises artesian-type freshwater seepage with episodic discharge at deep-water pockmarks such as MET1 (Szymczycha et al., 2018; Idczak et al., 2020). Deep SGD originates from extensive Upper Cretaceous aquifers beneath the Gulf of Gdańsk (Uścinowicz, 2011). Seepage intensity varies with hydrostatic pressure, water-column processes, and fault activity (Brodecka-Goluch et al., 2022). After commercial extraction ceased in 2000, natural hydrodynamic conditions returned (Uścinowicz, 2011), although the extent and periodicity of deep discharge remain unquantified. SGD in the MET1 area reduces sulphate and chloride concentrations with depth, thereby compressing the SMTZ to a few cm below the seafloor (Idczak et al., 2020; Brodecka-Goluch et al., 2022; Łukawska-Matuszewska and Dwornik, 2025). A high carbonate alkalinity flux at MET1-MP indicates substantial DIC generation during anaerobic diagenesis, potentially linked to Fe(III)-AOM (Łukawska-Matuszewska and Dwornik, 2025). The near-bottom chloride concentration in the Gulf of Gdańsk ranges from 150 to 180 mmol L^{-1}, equivalent to ~5318-6384 mg dm^{-3} (Lukawska-Matuszewska, 2016). For the Gdańsk Deep, the mean value is approximately 12 PSU, equivalent to 6700-6900 mg dm^{-3} (Kapustina et al., 2026).

2.2 Sampling at MET stations

The research stations were divided into pockmarks (morphologically concave geological structures with gas emissions to the water column and/or gas-bearing sediments with possible SGD) and references (non-pockmark reference sites with gas in the sediments but without emission to the water column or SGD). Pockmark stations were further classified (see supplementary material Table S1) based on previous studies, including hydroacoustic and geophysical investigations (Brodecka-Goluch et al., 2020, 2022; Idczak et al., 2020), as well as data included in this study (SO_4^{2-} and CH_4 profiles: Fig. 2; Cl^- profiles: Fig. 3; echograms for pockmarks MET3 and MET4: supplementary material Fig. S1), as active (gas emission to the water column, influence of freshened porewater, or both: P/MET1-BH, P/MET1-MP), weakly active (gas seepage and porewater freshening: P/MET4), or inactive (gas present in the sediments without clear emission or freshwater seepage: P/MET3).

Eight 95 cm-long sediment cores were collected from the central parts of methane-seeping structures in the central Gdańsk Basin (south-eastern Baltic Sea) using a gravity corer at three areas and four study locations (MET1: MET1-MP, MET1-BH; MET3; MET4; Fig. 1, supplementary material Table S1) during a cruise aboard RV *Oceanograf* (University of Gdańsk) in October 2019. Four additional cores were collected from outside the pockmarks (~100-150 m away) as reference samples. Samples were categorised by origin: a 'P' prefix (P/METX; X = 1-MP, 1-BH, 3, 4) for pockmark sediments and an 'S' prefix (S/METX) for surrounding sediments, namely reference non-pockmark sediments.

Onboard, the 95 cm cores for biomarker analysis were sectioned into a top 0-5 cm interval and subsequent 10 cm intervals (hereafter referred to as horizons) for the remainder of the cores, yielding 72 samples for geochemical analysis (some bottom samples are missing). Samples for microbial analysis were subsampled at a slightly coarser 10-cm resolution from the top (1), mid-depth (5), and bottom (7, 10) intervals using a sterile spatula.

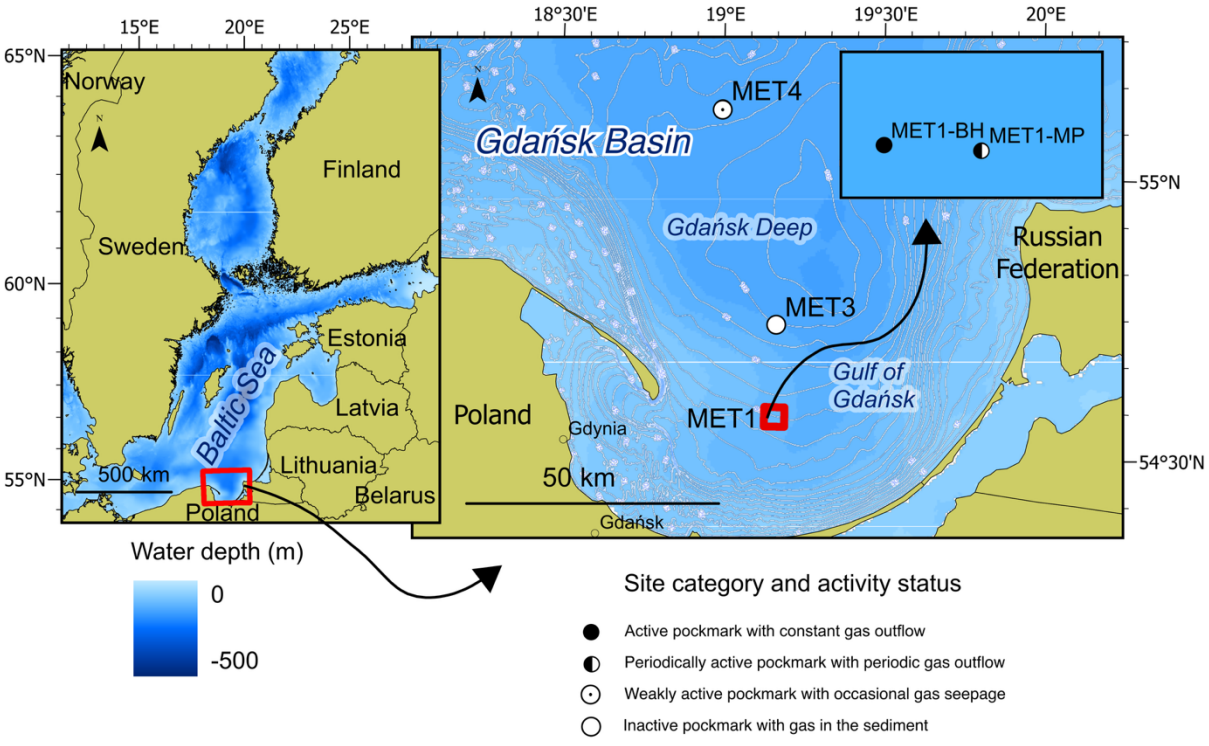

Fig. 1. Map of the study area in the south-eastern Baltic Sea, the Gdańsk Basin. The main panel shows the Gdańsk Basin, including the Gdańsk Deep and the Gulf of Gdańsk. Symbols indicate the category and activity status of the investigated pockmark sites (tagged with a "P" prefix) with respect to venting status, based on MBES and SBES observations collected during the present and previous research

campaigns in 2019-2025. Reference stations (labelled as surrounding stations and tagged with an "S" prefix) are referred to as non-pockmark cores or reference cores. They are positioned approximately 100-150 m from the corresponding pockmark margins on morphologically regular seafloor lacking pockmark depressions; they are not shown separately on the map due to the map's scale. Additional data, including CH_4/SO_4^{2-} profiles and Cl^- profiles, are presented in Figures 2 and 3, respectively. More detailed data, for example, concerning porewater freshening, are available in the supplementary material (Table S1). Map source: Eurostat/GISCO, 2024, scale 1.

2.3 Porewater sampling

Porewater samples were collected under anoxic conditions from intact, hermetically sealed sediment cores using Rhizon® samplers. Sediment subsamples for CH_4 determination were collected immediately after core retrieval. Sampling was performed through pre-drilled holes in the core liners using 3 mL syringes (with the Luer tip removed), and the material was immediately transferred into 20 mL vials in accordance with the protocol described by Jørgensen et al. (2001). Chloride and SO_4^{2-} concentrations in porewater were measured by high-performance ion chromatography (Metrohm 850 Professional IC) with analytical precision better than 3%. Methane concentrations were determined by the standard headspace technique using a gas chromatograph (Perkin-Elmer) equipped with a flame ionisation detector (FID) and an HP-5 capillary column (30 m × 0.32 mm × 0.25 µm), with helium as the carrier gas. The method detection limit (LOD) was 0.2 µmol dm^{-3}. Measured CH_4 concentrations were corrected for sediment porosity. Porosity for each sample was calculated from water and organic matter contents (LOI; see below) using the equations of Engvall (1978) and Carman and Jonsson (1991).

2.4 LOI analysis

The organic matter content was assessed by gravimetric loss-on-ignition (LOI) after dehydration (105 °C for 24 h) and dry combustion (550 °C for 6 h). Because LOI-derived organic matter estimates are sensitive to ignition conditions and sediment composition, and because mass loss at 550°C may include contributions from sediment mineralogy, including inorganic carbon-bearing minerals, LOI-based values provide only a screening-level estimate of total organic carbon (TOC) rather than an exact measurement. Therefore, LOI-based values were evaluated against directly measured TOC for two representative cores. TOC content in

sediments was measured using a CHNS autoanalyser (Perkin Elmer 2400) following Parsons et al. (1984). For TOC analysis, samples were acidified with 1 M HCl to remove inorganic carbon, following Hedges and Stern (1984). Due to the positive relationship between LOI and TOC in the selected cores from two study sites (n = 17; $R^2 = 0.43$; $p<0.005$), LOI was used as a high-resolution proxy for organic matter content, i.e., qualitatively (at the trend level) to provide geochemical context rather than for biomarker normalisation.

2.5 Tetraether lipid extraction and analysis

All freeze-dried samples were ground with a mortar and pestle. Approximately 1 g of each sample was extracted with dichloromethane:methanol (DCM:MeOH, 2:1, v/v) in an ultrasonic water bath. Total lipid extracts (TLEs) were chromatographed on a silica gel column with n-hexane and methanol as eluents to obtain apolar and polar fractions, respectively.

The polar fraction containing core GDGTs was re-dissolved in hexane/isopropanol (99:1, v/v), spiked with a known amount of an internal standard (a C_{46} glycerol trialkyl glycerol tetraether; Huguet et al., 2006), and filtered through a 0.45 µm polytetrafluoroethylene syringe filter. GDGTs were analysed at Utrecht University using an ultra-high-performance liquid chromatograph (UHPLC; Agilent 1260 Infinity) coupled to an Agilent 6130 single-quadrupole mass detector, following the method proposed by Hopmans et al. (2016). Quantification was performed by manually integrating the peak areas of the protonated ions ($[M+H]^+$) in ChemStation software (B.04.03), and the results were compared with those of the internal standard. Selected ion monitoring (SIM) was used to detect and identify GDGTs. The target ions were *m*/*z* 1302, 1300, 1298, 1296 and 1292 for iGDGTs and OH-GDGTs.

Absolute GDGT concentrations were calculated relative to the C_{46} internal standard and sediment dry weight, following established GDGT quantification approaches (Huguet et al., 2006, 2010), and are therefore reported as semi-quantitative concentrations (Bijl et al., 2025). Derived fractional abundances and GDGT-based indices were calculated from the integrated peak areas. Raw peak areas, derived fractional abundances and indices, and semi-quantitative absolute concentrations are reported in accordance with the GDGT data-reporting recommendations of Bijl et al. (2025).

Each sediment horizon was analysed once. Replicate analyses were not available for individual horizons. Therefore, sample-specific analytical uncertainty could not be estimated, and error

bars are not shown in the downcore plots. Method uncertainty includes peak integration, instrumental response, extraction/processing effects, and the semi-quantitative nature of C_{46}-based concentration estimates (Bijl et al., 2025).

2.6 DNA isolation, sequencing, and data analysis

Genomic DNA from the sediment samples was isolated using the EURx kit for complex matrices (Soil DNA Purification Kit, no. E3570, EURX Ltd., Poland). The protocol requires mechanical homogenisation to release cells from the sediment matrix. The isolated genomic DNA was subjected to metabarcoding analysis. Sequencing of the hypervariable V3–V4 region of the 16S rRNA gene was outsourced to GENOMED S.A. (Warsaw, Poland). Specific primer sequences (developed by Zymo Research, CA, USA) were used to amplify the selected region and prepare libraries (341F: CCTACGGGDGGCWGCAG, CCTAYGGGGYGCWGCAG; 806R: GACTACNVGGGTMTCTAATCC).

PCR was performed using Q5 Hot Start High-Fidelity 2× Master Mix, with reaction conditions in accordance with the manufacturer's recommendations. Sequencing was performed on a MiSeq sequencer using paired-end (PE) technology (2 × 300 nt) with Illumina's v3 kit. FASTQ files were processed with *fastp* (v. 0.23.2) (Chen et al., 2018) to improve raw sequence quality by trimming adapters, filtering low-quality reads, and removing artefacts. The sequences were further analysed using Kraken2 (Wood et al., 2019) following the protocol described by Lu et al. (2022). The SILVA database (v. 138) was used for taxonomic assignment (Quast et al., 2013). Bracken was then applied to the Kraken2 reports, set to the genus level with a threshold of five (Lu et al., 2017). The resulting data were transformed before analysis. To address zero values, the data were imputed using the R package *Compositions* (v. 1.4.0.1) (Palarea-Albaladejo and Martín-Fernández, 2015). The centred log-ratio (clr) transformation was then applied using the *Compositions* package for R (v. 2.05; Aitchison, 1982; Quinn et al., 2019; van den Boogaart et al., 2024).

Taxonomic names are reported according to the database classification used in the bioinformatic workflow. The Deep Sea Euryarchaeotic Group (DSEG) is therefore retained when returned by the database, although this lineage is classified within Thermoplasmatota in newer phylogenetic classifications (Rinke et al., 2021).

2.7 Statistical analysis and data visualisation

Multidimensional analyses, correlograms, and hierarchical analyses were conducted using R (R Core Team, 2023). RStudio 2025.05.0+496 “Mariposa Orchid” and R version 4.3.3 (2024-02-29) on the x86_64-apple-darwin20 (64-bit) platform were used for all analyses. A heatmap of the archaeal community (at the class level) with cluster analysis was generated using the Heatmap function in the *ComplexHeatmap* package. To examine the grouping of samples between pockmark and reference sites, Classical Multidimensional Scaling (MDS; principal coordinates analysis) was performed using the dist function (dist_matrix <- dist(data), method = "euclidean") and the cmdscale function (mds <- cmdscale(dist_matrix)) from the *stats* package. The MDS results were visualised using the *ggplot2* and *ggrepel* packages (Wickham, 2016).

Permutational Multivariate Analysis of Variance (PERMANOVA) was conducted using adonis2 (permutations = 999, method = "bray") in the *vegan* package. Principal Component Analysis (PCA) was conducted using the *FactoMineR* package, and the results were visualised with fviz_pca_var from the *factoextra* package. A correlation network illustrating relationships between Archaea (at the family taxonomic level) and GDGTs was constructed using *cor* from the *stats* package; graph_from_adjacency_matrix (mode = "undirected", weighted = TRUE, diag = FALSE) from the *igraph* package; mutate_as_tbl from the *tidygraph* package; and *ggraph* for visualisation. Community structure was identified using group_louvain (multilevel optimisation of modularity via igraph::cluster_louvain()), which implements the multi-level modularity optimisation algorithm described by Blondel et al. (2008). Cross-correlations between iGDGT and OH-GDGT concentrations were calculated in R using stats::cor.test() with Pearson correlation. Concentrations were $\log_{10}$-transformed ($\log_{10}[x + 10^{-6}]$) before correlation analysis to reduce right skew. Correlations were computed using pairwise complete observations. To correct for multiple testing, *p*-values were adjusted using the Benjamini–Hochberg false discovery rate (FDR) procedure.

2.8 Calculation of indices

The GDGT-0/crenarchaeol ratio was calculated to assess potential contributions to iGDGT production from methanogens (although GDGT-0 is not exclusive to them) and ammonia-oxidising archaea (Blaga et al., 2009). Values > 2 have been proposed to indicate a substantial methanogenic input (Blaga et al., 2009; Schouten et al., 2013; Zell et al., 2014).

GDGT-0/cren = [GDGT-0] / [crenarchaeol]

The GDGT-2/crenarchaeol (GDGT-2/cren) index is used as an additional screening tool to assess a potential AOM contribution (Weijers et al., 2011). An elevated GDGT-2/cren ratio suggests increased synthesis of GDGT-2 within the SMTZ, likely from methanotrophic Euryarchaeota (Pancost et al., 2001; Wakeham et al., 2003; Stadnitskaia et al., 2005).

GDGT-2/cren = [GDGT-2] / [crenarchaeol]

The Methane Index (MI) is based on GDGT-1 to GDGT-3 and crenarchaeol, and reflects the balance between methanotrophic Euryarchaeota and Nitrososphaeria, whether planktonic or benthic (Zhang et al., 2011). GDGTs associated with methanotrophs — mainly GDGT-1 to GDGT-3 (Pancost et al., 2001; Zhang et al., 2011) — are primarily produced by ANME-1 (Rossel et al., 2008). The MI ranges from 0 to 1, with higher values (>0.3-0.5) indicating a greater relative contribution of GDGT-1 to GDGT-3 than of crenarchaeol and cren', and are linked to high methane fluxes (Kim and Zhang, 2023). The MI, as defined by Zhang et al. (2011), was calculated as follows:

MI = [GDGT-1 + GDGT-2 + GDGT-3] / [GDGT-1 + GDGT-2 + GDGT-3 + cren + cren′]

The Branched and Isoprenoid Tetraether index (BIT) estimates the relative contribution of branched GDGTs to the combined pool of branched GDGTs and crenarchaeol, following Hopmans et al. (2004), and serves as an indicator of terrestrial organic matter input into a marine environment. However, brGDGTs may also be produced in situ in aquatic and sedimentary environments (Peterse et al., 2009; Dearing Crampton-Flood et al., 2019 and references therein). The BIT index ranges from 0 to 1, with higher values indicating a greater relative contribution of brGDGTs compared with crenarchaeol:

BIT = [brGDGT-Ia + II-a + IIIa] / [br-GDGT-Ia + IIa + IIIa + cren]

The percentage of OH-GDGTs reflects the relative contribution of hydroxylated iGDGTs to the total iGDGT pool and indicates an increased contribution from OH-GDGT–producing archaea and/or adaptation to low temperature and salinity. The index was calculated following Huguet et al. (2013):

OH-GDGT% = Σ[OH-GDGT-0 + OH-GDGT-1 + OH-GDGT-2] / {Σ[OH-GDGT-0 + OH-GDGT-1 + OH-GDGT-2] + Σ[GDGT-0 + GDGT-1 + GDGT-2 + GDGT-3 + cren + cren′]} × 100

The ring indices of hydroxylated tetraethers (RI-OH and RI-OH′) quantify the degree of cyclisation, that is, the number of cyclopentane rings in the molecules. This number increases with temperature and decreases with salinity (Sinninghe Damsté et al., 2022). The RI-OH′ is more sensitive in cold regions (Varma et al., 2024). The indices were calculated following Lü et al. (2015):

$$RI\text{-}OH = \{[OH\text{-}GDGT\text{-}1] + 2 \times [OH\text{-}GDGT\text{-}2]\} / \{[OH\text{-}GDGT\text{-}1] + [OH\text{-}GDGT\text{-}2]\}$$

$$RI\text{-}OH' = \{[OH\text{-}GDGT\text{-}1] + 2 \times [OH\text{-}GDGT\text{-}2]\} / \Sigma[OH\text{-}GDGTs]$$

3 Results

3.1 Porewater profiles of SO_4^{2-}, CH_4, and Cl^-

Pockmarks across all sites show greater sulphate depletion, with a mean SO_4^{2-} concentration 1.5× lower than in non-pockmarks (244.4 ± 371.0 SD mg dm^{-3} vs 377.5 ± 364.4 SD mg dm^{-3}, respectively, Fig. 2). Although SO_4^{2-} concentrations span similar value ranges in pockmarks and non-pockmarks (3.1–992 mg dm^{-3} vs 6.6–1031 mg dm^{-3}, respectively), their median values differ substantially by a factor of ~5 (40.9 vs 200 mg dm^{-3}, respectively). Pockmarks also show SO_4^{2-} depletion occurring closer to the surface, meaning the depth at which SO_4^{2-} first drops below 100 mg dm^{-3} (at 17.3 ± 5.9 cm in pockmark cores compared with 36.3 ± 23.5 cm in reference cores) and 50 mg dm^{-3} (17.3 ± 5.9 cm in pockmark cores compared with 497.7 ± 27.8 cm in reference cores) is 2 and 3× shallower, respectively. Pockmarks show mean CH_4 concentrations 2.3-fold higher than at reference sites (3.1 ± 2.6 mM vs 1.3 ± 1.4 mM, mean ± SD; Fig. 2). Median CH_4 concentrations were also higher in pockmark-cores (2.24 vs 1.44 mM), reflecting the influence of particularly high CH_4 concentrations in selected pockmark horizons. MET4 exhibits the most extreme values across the examined sites and the greatest differences between pockmark and reference cores; CH_4 reached the highest values in the pockmark core, whereas the reference core remained close to CH_4-free. By contrast, MET3 shows the least differentiation between pockmark and reference cores and has lower overall methane concentrations.

Sulphate and CH_4 show clear, opposing depth trends across all four study locations, except at non-methane MET4, where CH_4 is absent, and sulphate is high throughout the profile (Fig. 2). SO_4^{2-} is initially high in surface sediments and declines with depth, whereas CH_4 shows the opposite pattern. Based on the definition of the SMTZ as the depth where porewater SO_4^{2-} and

CH_4 concentrations oppose each other, this pattern may indicate the SMTZ location. However, the magnitude and depth of these changes, as well as differences between pockmark and reference sites, vary by location. Midpoints ranged from 10–15 cm in pockmark sediments and 10–45 cm in non-pockmark sediments, suggesting a shallower SMTZ in pockmarks than in reference non-pockmarks of MET1-BH and MET3, a similarly shallow SMTZ in MET1-MP, and no SMTZ in the sampled interval of non-pockmark MET4.

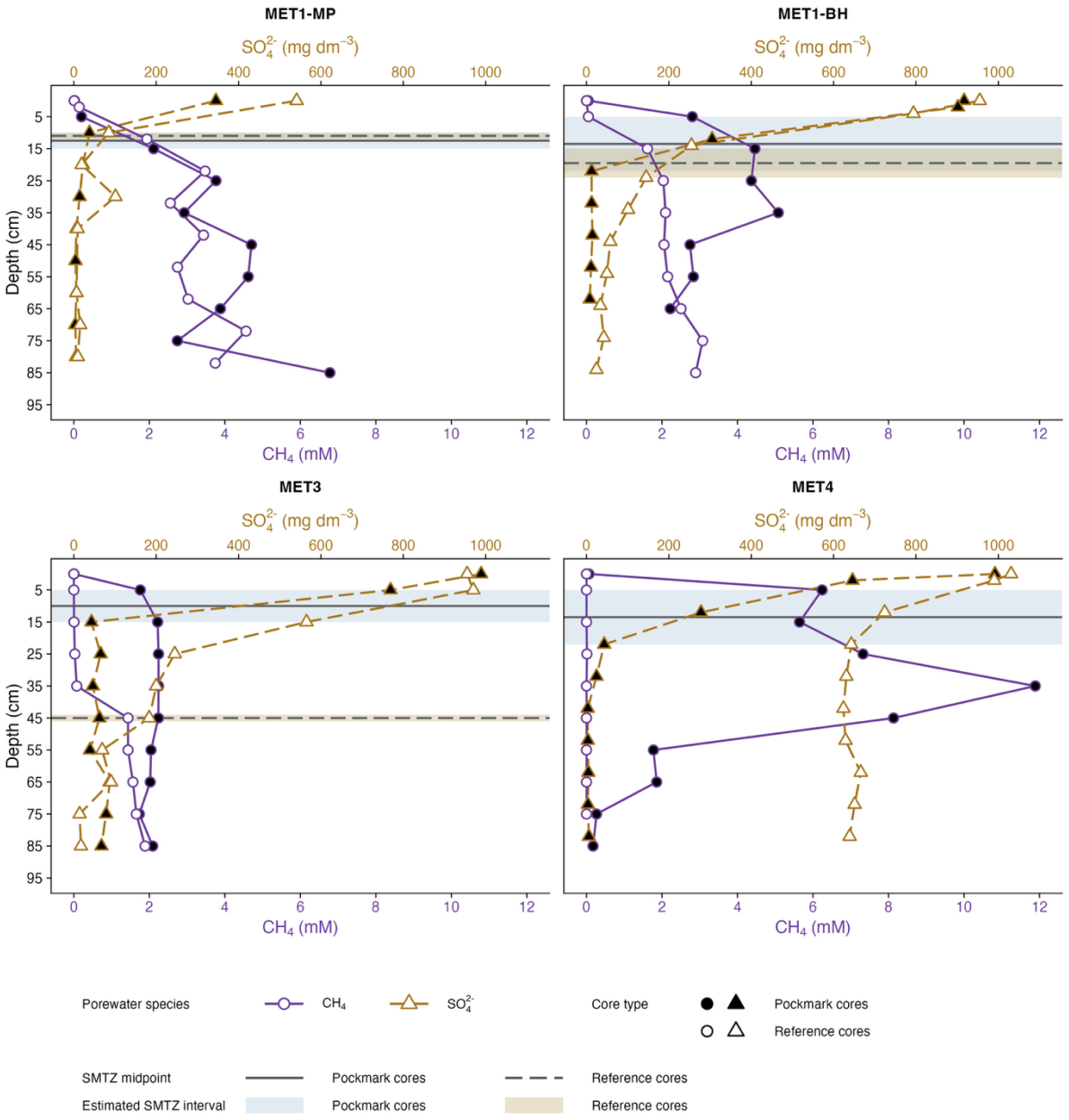

Fig. 2. Profiles of sulphate and methane differ in absolute concentrations across sites. The bands representing the SMTZ width in the sulphate and methane profile plots were defined by two criteria: where sulphate declines to ≤ 20% of its surface value, and where methane becomes detectably present, defined as ≥ 20% of the maximum value in each profile (with a minimum threshold of 0.1 mM). Dashed

(reference cores) and solid (pockmark cores) horizontal lines indicate the midpoint of the estimated SMTZ.

Chloride porewater profiles differed among the investigated sites, with generally lower concentrations in pockmark cores than in reference cores (Fig. 3). Across the sediment-depth intervals, Cl^- concentrations averaged 6198 ± 645 mg dm^{-3} in reference cores and 5367 ± 1089 mg dm^{-3} in pockmark cores.

The strongest contrast between the pockmark and reference cores is evident at MET4 (Fig. 3). This contrast reflects a pronounced downcore Cl^- depletion in the MET4 pockmark core (from 6927 mg dm^{-3} at the surface to 4182-4490 mg dm^{-3} below 50 cm depth), compared with the reference core, which shows consistently higher and steady chloride concentrations (6060-7279 mg dm^{-3}). This pattern indicates freshwater enrichment within the MET4 pockmark core relative to the adjacent reference core. However, the lowest concentrations occur in the MET1-MP pockmark core, where Cl^- decreases steadily with depth (from 5938 mg dm^{-3} at the surface to 2863 mg dm^{-3} at the bottom of the core). Whereas Cl^- concentrations also decrease with depth in the reference core of MET1-MP, they remain higher than in the MET1-MP pockmark core (Fig. 3). In the MET1-BH pockmark core, Cl^- concentrations are lower than in the reference core throughout the sediment profile, but the pattern is irregular (a dip to 4667 mg dm^{-3} at 20 cm and a recovery to ~5200-5600 mg dm^{-3} below). In the MET1-BH reference core, Cl^- concentrations are higher and more variable (5512-6838 mg dm^{-3}). At MET3, the pockmark and reference cores are largely similar across the depth profile and remain among the highest Cl^- levels in the dataset. The main difference appears in the deepest MET3 pockmark sample, where the chloride concentration drops (4781 mg dm^{-3} at 85 cm), whereas the reference core remains stable (6192-7015 mg dm^{-3}) (Fig. 3).

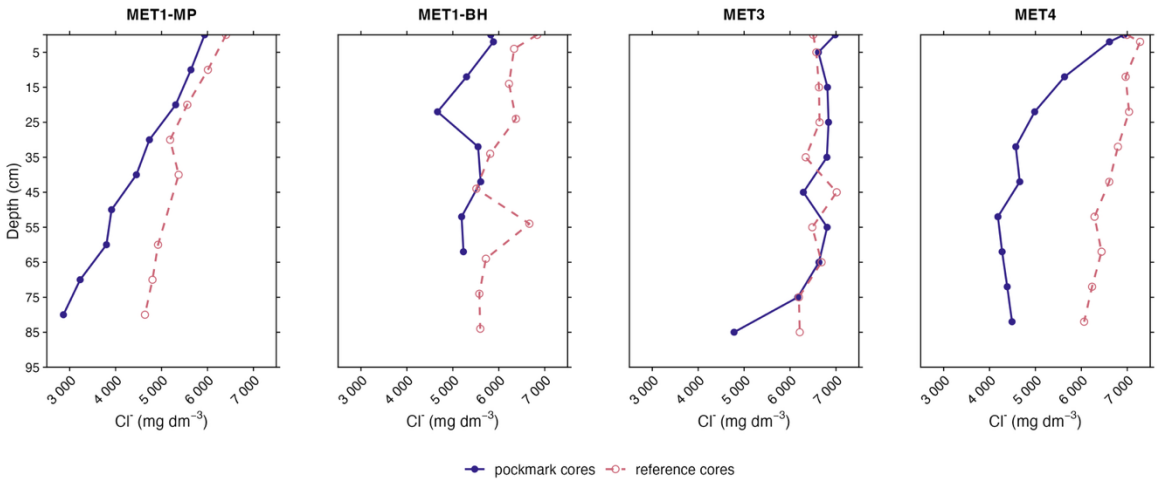

Fig. 3. Depth profiles of porewater chloride (Cl^-) at MET1-MP, MET1-BH, MET3, and MET4, ranging from 2863 to 7279 mg dm^{-3}. The profiles consistently show higher chloride concentrations in reference sediments than in pockmark sediments. The extent and shape of these profiles vary among sites. The most distinct separation between pockmark and reference profiles occurs at MET4 and MET1-MP, whereas MET3 shows substantial overlap. Depth is given in cm below sea floor (bsf).

3.2 LOI

To assess whether LOI captured the main downcore stratigraphic trends in organic carbon, LOI profiles were compared with directly measured TOC in two representative cores: the MET1-MP pockmark core and the MET3 reference core (Fig. 4). Across these samples, LOI and measured TOC showed a positive relationship ($n = 17$, $R^2 = 0.43$, $p = 0.004$), supporting the use of LOI as a proxy for organic matter variability. In both cores, intervals of increased LOI consistently coincide with higher measured TOC, demonstrating that LOI reliably reflects variations in organic matter content, despite differences in absolute values.

In the MET1-MP pockmark core, both LOI and measured TOC are relatively elevated in the upper to middle part of the core and generally decrease below ~45-55 cm depth (Fig. 4). This indicates a downcore decline in bulk organic matter content below the mid-core interval. In the MET3 reference core, measured TOC is highest in the shallowest interval and decreases through the upper-middle section of the core, while LOI follows a comparable vertical pattern (Fig. 4). Therefore, LOI is used below as a qualitative, high-resolution proxy for bulk organic matter trends in the studied cores, providing a sedimentary and geochemical context for the GDGT and microbial distributions.

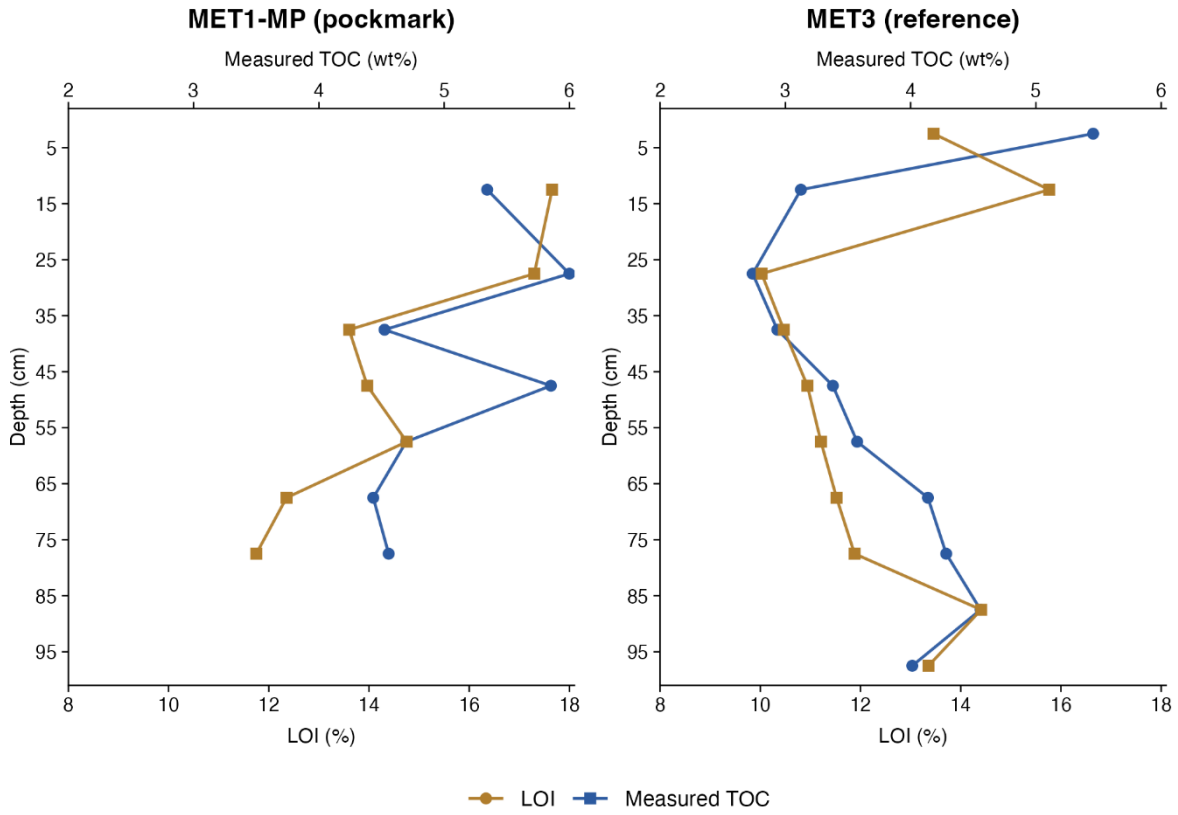

Fig. 4. Comparison of loss-on-ignition values (LOI%, lower x-axis) and directly measured total organic carbon (TOC wt%, upper x-axis) in two representative sediment cores from the south-eastern Baltic Sea: the MET1-MP pockmark core from the Gulf of Gdańsk and the MET3 reference core from the Gdańsk Deep. Both parameters are plotted against sediment depth (cm bsf). This comparison was used to assess whether LOI captures the main stratigraphic variability in organic matter content. Across both cores, LOI and measured TOC show a positive correlation (n = 17, $R^2 = 0.43$, $p = 0.004$), supporting the use of LOI as a qualitative, trend-level proxy for variability in bulk organic matter. Although sample-scale offsets occur between LOI and TOC, the profiles broadly reproduce comparable downcore patterns.

LOI values show site-specific and downcore variability, with varying degrees of contrast between pockmark and reference cores, indicating differences in bulk organic matter content and relative enrichment in pockmark cores, especially pronounced in MET1-BH (Fig. 5). In the MET1 area, the same reference core was used for comparison with the MET1-MP and MET1-BH pockmarks. LOI values were elevated in selected pockmark cores compared with reference cores, particularly in MET1-BH and MET1-MP, with LOI values on average approximately 2.3-fold higher in the MET1-BH pockmark core and 1.4-fold higher in the MET1-MP pockmark core relative to the shared MET1 reference core. The strongest enrichment occurs at

MET1-BH, where pockmark LOI values are about 1.9-3.0 times higher than the corresponding reference values. In contrast, pockmark MET3 shows only a weak average difference of ~1.1-fold, with depth-wise ratios ranging from 0.7 to 1.3, indicating that LOI values are broadly overlapping between pockmark and reference cores.

At MET4, pockmark LOI values were on average ca. 1.4-fold higher than in the reference core, with the relative difference increasing downcore and reaching approximately 2.1-fold in the deepest interval of the profile, where the reference core shows low LOI values of ~4% (Fig. 5). The LOI results, used as a proxy for organic matter content, indicate that organic matter accumulation is site-specific and should not be generalised across all pockmarks.

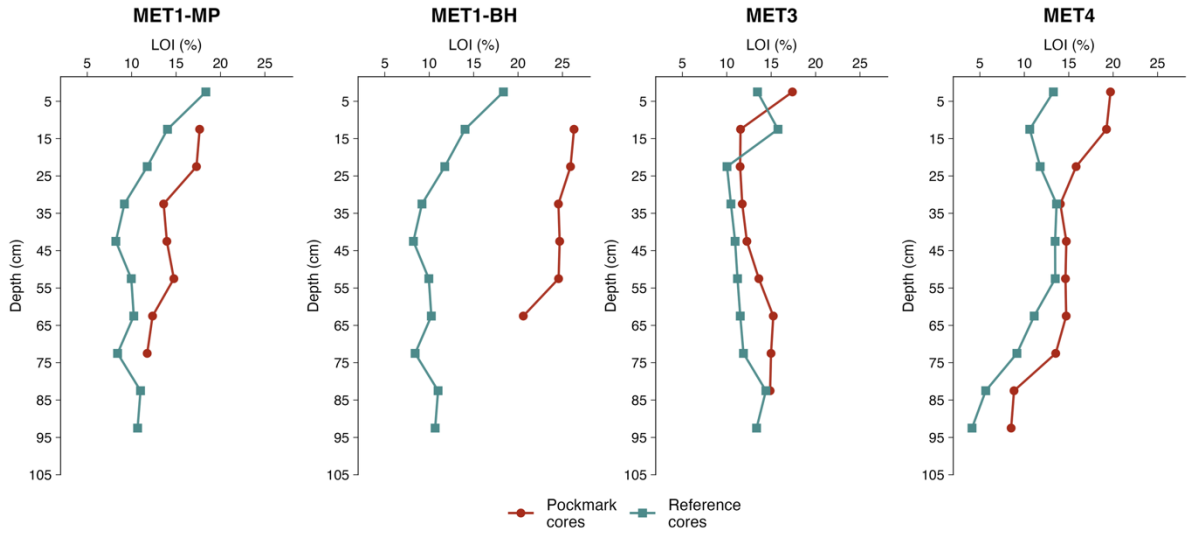

Fig. 5. Downcore variation of loss-on-ignition (LOI%) in sediment cores collected from the Gulf of Gdańsk (MET1-MP, MET1-BH) and the Gdańsk Deep (MET3, MET4), south-eastern Baltic Sea. LOI values are plotted against depth bsf (cm) and serve as a qualitative, screening-level proxy for variability in bulk organic matter. Pockmark sediments are compared with adjacent reference (non-pockmark) sediment cores at each site; for the MET1-MP and MET1-BH pockmarks, the same reference core is used. LOI values are elevated in the pockmark cores at MET1-MP, MET1-BH, and MET4, with the strongest enrichment observed at MET1-BH. By contrast, MET3 shows values that are approximately overlapping between the pockmark and reference sediment cores. At MET4, both cores show a pronounced downcore decrease in LOI, particularly in the reference core, where values decline to ca. 4% in the deepest part of the profile.

3.3 iGDGTs in pockmark and non-pockmark marine surface sediments

The abundance and distribution of iGDGTs (GDGT-0 to GDGT-3, crenarchaeol, and its isomer) were analysed in pockmark core sediments and in surrounding non-pockmark reference core sediments (Fig. 6). All targeted iGDGTs were detected in both settings.

Unless stated otherwise, concentration values are reported as ranges, followed by the median and the mean ± standard deviation (SD). Summed iGDGT concentrations (ΣiGDGTs) span 0.02–58.85 μg g^{-1} sediment across all samples, with values generally higher and more variable in pockmark sediment cores (0.92–58.85 μg g^{-1} sediment; 5.10 μg g^{-1}; 10.58 ± 13.08 μg g^{-1}) than in reference sediment cores (0.02–16.81 μg g^{-1} sediment; 2.59 μg g^{-1}; 3.73 ± 3.41 μg g^{-1}), that is, approximately twice the median and three times the mean. Spatially, the highest ΣiGDGT concentrations occur at sites in the Gdańsk Deep (MET3, MET4), whereas lower concentrations are generally observed in the MET1 area (Fig. 6). With depth, ΣiGDGTs commonly show shallow to mid-depth maxima, particularly between approximately 15 and 45 cm bsf, followed by downcore depletion. Excluding the anomalously low values in the S/MET4 reference core, ΣiGDGTs concentrations typically decline by a factor of ~2.6 to ~64, although the fold decrease is much larger where the deepest reference intervals approach near-zero values in S/MET4.

Crenarchaeol (cren) is the dominant iGDGT in both pockmark cores (mean fractional abundance of 0.53 ± 0.03 SD) and reference cores (0.55 ± 0.02 SD) (Fig. 7). GDGT-0 is the second most abundant in pockmark and reference cores (0.43 ± 0.03 SD; 0.41 ± 0.02 SD, respectively) (Fig. 7). Together, crenarchaeol and GDGT-0 account for ~96 % of the total iGDGT pool in both pockmark and reference cores, indicating broadly similar iGDGT distributions between pockmarks and references. Consistently, GDGT-0 covaries very strongly with crenarchaeol ($r = 0.996$, $p < 0.001$).

The remaining iGDGTs, GDGT-1 to GDGT-3, occur only in minor proportions and at much lower concentrations (Fig. 7). Across the analysed depth intervals from 0-5 to 90-95 cm bsf, GDGT-1, GDGT-2, and GDGT-3 show a highly consistent pattern of relative abundance. In 74 of 75 samples, the order is GDGT-1 > GDGT-2 > GDGT-3, and GDGT-2 is not the dominant compound in any sample. The only exception is sample P/MET4/3, where the order is GDGT-1 > GDGT-3 > GDGT-2.

Concentration profiles of the individual iGDGTs (Supplementary material Fig. S2) generally follow similar downcore patterns, except for isolated concentration maxima of GDGT-1 in

P/MET1-BH/6 and GDGT-3 in P/MET4/3, minor changes in the crenarchaeol isomer (cren′) at MET1-MP and MET1-BH, and even smaller differences at MET3 and MET4. GDGT-1, GDGT-2, and GDGT-3 also show strong covariation with crenarchaeol (r = 0.988, 0.954, 0.951, $p < 0.001$). Across all iGDGT pairs, correlations are consistently strong (r = 0.847–0.996, $p < 0.001$), indicating that the individual iGDGTs vary largely in concert rather than exhibiting compound-specific enrichments.

The mean ± SD values for the indices are reported in Table 1. The GDGT-0/cren ratio is moderate and broadly comparable between pockmark and reference cores, ranging from 0.65 to 0.99 in pockmark cores and from 0.63 to 0.91 in reference cores. No consistent downcore trend is observed across all cores; where changes occur, they are site-specific and modest relative to the overlap between pockmark and reference cores. The GDGT-2/cren ratio is consistently low (0.01–0.04), and MI values remain low, ranging from 0.04 to 0.09 in pockmarks and from 0.03 to 0.07 in references. The BIT index values are generally low, ranging from 0.008 to 0.143 in pockmarks and from 0.034 to 0.468 in references, with the slightly higher values (negligible) confined mainly to the deepest intervals of the MET4 reference core.

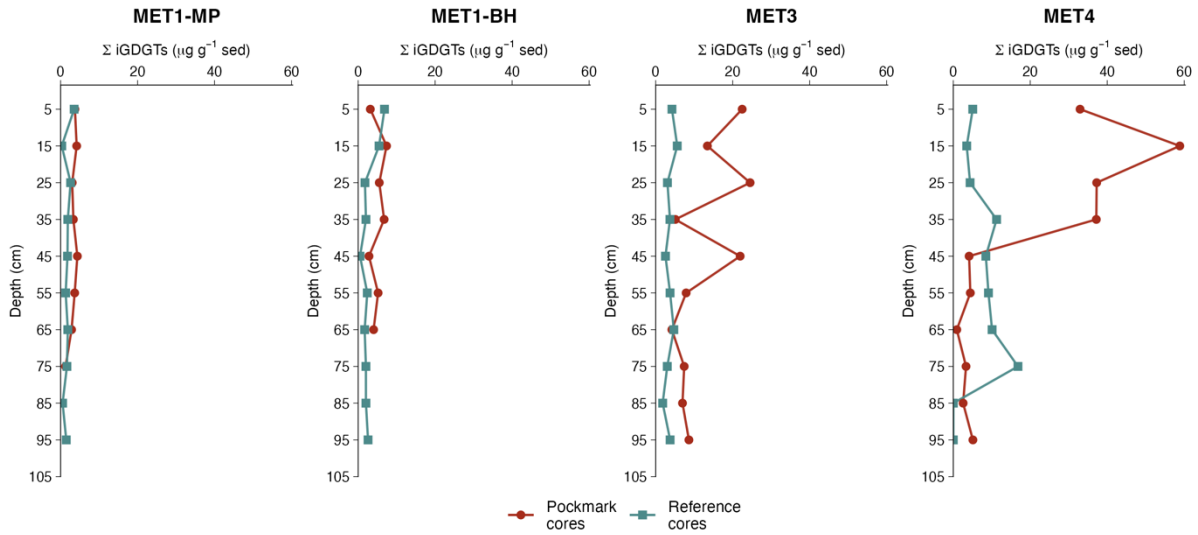

Fig. 6. Downcore profiles of summed isoprenoidal glycerol dialkyl glycerol tetraethers (ΣiGDGTs; μg g^{-1} dry sediment) for sediment cores from four sites in the south-eastern Baltic Sea: MET1-MP and MET1-BH (Gulf of Gdańsk), and MET3 and MET4 (Gdańsk Deep). Concentrations are plotted as a function of depth below the sea floor (cm bsf), showing a general downcore decrease. ΣiGDGTs exhibit elevated concentrations in pockmark sediment cores relative to adjacent reference sediment cores, with the most pronounced enrichment observed at the Gdańsk Deep sites (MET3, MET4), where elevated near-surface values are followed by a downcore decrease. Error bars are not shown because each point represents a single sediment horizon analysed once (see section 2.5).

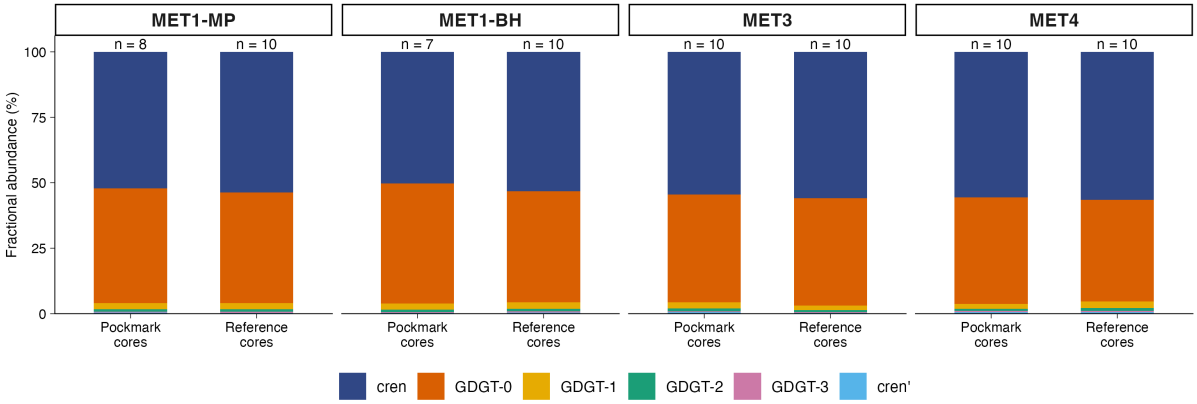

Fig. 7. Mean fractional abundances of iGDGTs in pockmark and reference cores at sites MET1-MP, MET1-BH, MET3, and MET4 in the south-eastern Baltic Sea. Stacked bars show mean fractional abundances of iGDGTs (GDGT-0–3, crenarchaeol, and cren′), averaged by site and core type; n indicates the number of horizons (samples). The upper panel shows the full scale (0–100%). Crenarchaeol and GDGT-0 dominate across all sites, whereas GDGT-1–3 and cren′ constitute minor fractions.

Table 1. Mean GDGT-based indices for pockmark (P) and reference (S) sediment cores at MET1 (MP, BH), MET3, and MET4. Values are reported as mean ± sample standard deviation, rounded to a maximum of two significant figures. Metrics include OH-GDGT%, hydroxylated GDGT ring indices (RI-OH, RI-OH′), the Branched and Isoprenoid tetraether index (BIT), the Methane Index (MI), and diagnostic ratios (GDGT-0/cren, GDGT-2/cren). RI-OH shows minimal variation across sites and between pockmark and reference cores (~1.1–1.2), indicating comparable OH-GDGT cyclisation patterns. OH-GDGT% is moderately elevated at MET1 relative to MET3–MET4, with minimal within-site variation. MI values remain consistently low (0.05–0.07). GDGT-0/cren ratios are consistently slightly elevated in pockmark cores relative to paired references, whereas GDGT-2/cren remains uniformly low (0.01–0.02), indicating that pockmark influence primarily affects GDGT-0 abundance rather than higher-cyclised GDGTs.

Sediment core	OH-GDGT%	RI-OH	RI-OH'	BIT	MI	GDGT-0/cren	GDGT-2/cren
P/MET1-MP	9.0±0.4	1.2±0.03	0.19±0.02	0.12±0.01	0.065±0.003	0.84±0.02	0.019±0.001
P/MET1-BH	9.3±0.4	1.2±0.04	0.19±0.02	0.09±0.01	0.066±0.003	0.92±0.04	0.019±0.002
P/MET3	7.9±0.9	1.2±0.02	0.21±0.03	0.05±0.02	0.064±0.008	0.76±0.11	0.021±0.004
P/MET4	7.8±1.3	1.1±0.02	0.19±0.02	0.03±0.02	0.054±0.016	0.74±0.08	0.014±0.003
S/MET1-MP	8.1±0.8	1.2±0.04	0.25±0.04	0.14±0.03	0.066±0.002	0.79±0.05	0.019±0.001
S/MET1-BH	8.1±0.9	1.2±0.02	0.23±0.03	0.12±0.02	0.066±0.003	0.80±0.06	0.019±0.001

S/MET3	7.0±0.6	1.2±0.03	0.19±0.02	0.07±0.01	0.047±0.003	0.73±0.07	0.013±0.001
S/MET4	7.2±0.9	1.2±0.06	0.21±0.07	0.13±0.16	0.065±0.036	0.69±0.03	0.019±0.013

620

621 **3.4 OH-GDGTs in pockmark and non-pockmark sediments**

622 The abundance and distribution of hydroxylated GDGTs (OH-GDGT-0 to -2) in pockmark and
623 reference cores broadly mirror those of iGDGTs, with strong positive cross-correlations (r =
624 0.840–0.992, $p < 0.001$) and the tightest coupling with GDGT-0 (ΣOH-GDGTs: $r = 0.992$, $p <$
625 0.001) and crenarchaeol ($r = 0.983$, $p < 0.01$). All targeted OH-GDGTs (OH-GDGT-0 to -2)
626 were detected in both settings.

627 Summed OH-GDGT concentrations (ΣOH-GDGTs) ranged from 0.00 to 6.30 μg g^{-1} sediment
628 across all samples, with values generally higher in pockmark sediment cores (0.06–6.30 μg g^{-1}
629 sediment; 0.43 μg g^{-1} sediment; 1.02 ± 1.36 μg g^{-1} sediment) than in reference sediment cores
630 (0.00–1.75 μg g^{-1} sediment; 0.21 μg g^{-1} sediment; 0.31 ± 0.32 μg g^{-1} sediment) (Fig. 8). ΣOH-
631 GDGTs are therefore, on average, approximately three times higher and, at the median, about
632 twice as high in pockmarks as in references. Spatially, the highest ΣOH-GDGTs concentrations
633 occur at MET4, intermediate values at MET3, and lower values in the MET1 area, broadly
634 mirroring the spatial pattern observed for ΣiGDGTs. With depth, ΣOH-GDGTs commonly
635 show shallow to mid-depth maxima, typically between 15 and 45 cm bsf, followed by downcore
636 depletion (Fig. 8). This decrease is particularly pronounced at MET4, especially in P/MET4,
637 where ΣiGDGTs declined from 6.30 to 0.06 μg g^{-1} sediment.

638 Across all cores, OH-GDGTs are dominated by OH-GDGT-0 in both pockmark and reference
639 cores (Fig. 9, average fractional abundances of 0.83 ± 0.02 SD and 0.82 ± 0.03 SD, respectively).
640 OH-GDGT-1 and OH-GDGT-2 are consistently minor components (Fig. 9). Overall, OH-
641 GDGT distributions are broadly similar between pockmark and reference cores (Supplementary
642 material Fig. S4), and most variability is evident in downcore concentration profiles, which
643 typically decline by a factor of ~1.2 to ~7.8, with most cores showing an average decrease by a
644 factor of ~3 (except for S/MET4, which declines to zero at the base). Across all OH-GDGT
645 pairs (OH-0, OH-1, OH-2), correlations are consistently very strong ($r = 0.975$–0.992, $p < 0.01$).

646 OH-GDGT% and RI-OH show only minor differences between pockmark and reference cores
647 (Table 1). OH-GDGT% values are slightly higher in pockmarks (6.4–9.9) than in references
648 (6.2–9.4). RI-OH is identical between settings (1.1–1.3 in pockmarks; 1.1–1.3 in references),

whereas RI-OH′ is modestly higher in references (0.16–0.36) than in pockmarks (0.16–0.25). Overall, variability in OH-GDGTs is mainly reflected in absolute abundances, while OH-GDGT distribution and indices are broadly comparable between pockmark and reference cores.

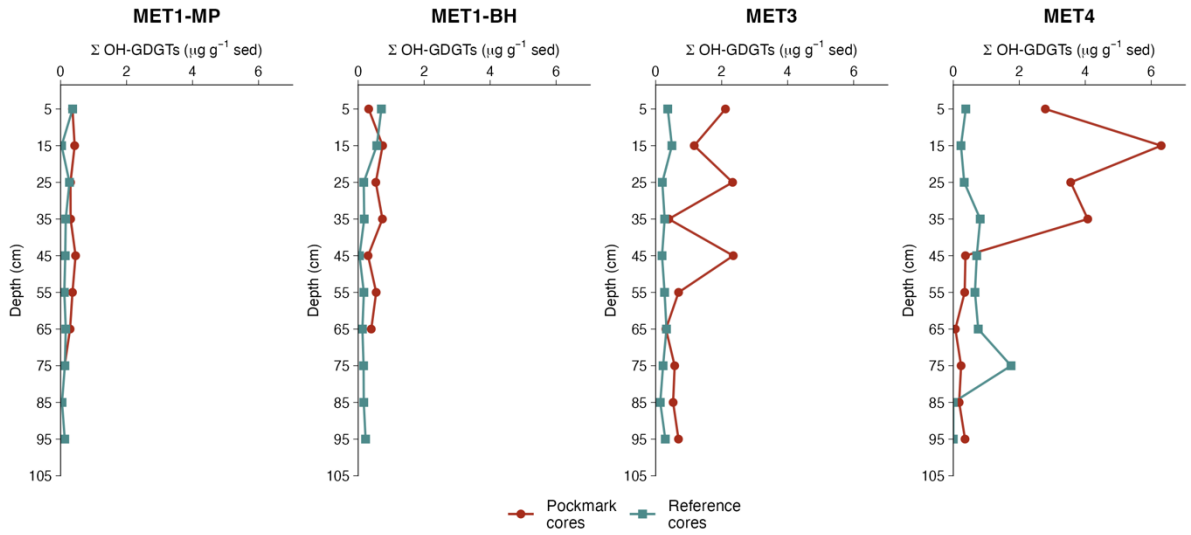

Fig. 8. Downcore profiles of summed hydroxylated glycerol dialkyl glycerol tetraethers (ΣOH-GDGTs; µg g^{-1} dry sediment) for sediment cores from four sites in the south-eastern Baltic Sea: MET1-MP and MET1-BH (Gulf of Gdańsk) and MET3 and MET4 (Gdańsk Deep). Concentrations are plotted against depth (downcore increase; cm). ΣOH-GDGT concentrations follow the pattern of iGDGTs, showing strong positive cross-correlations and the highest coupling with GDGT-0 and crenarchaeol (see Section 3.2). In the Gulf of Gdańsk (MET1-MP, MET1-BH), ΣOH-GDGTs show lower overall abundances than iGDGTs but remain elevated in pockmark intervals relative to reference sediments.

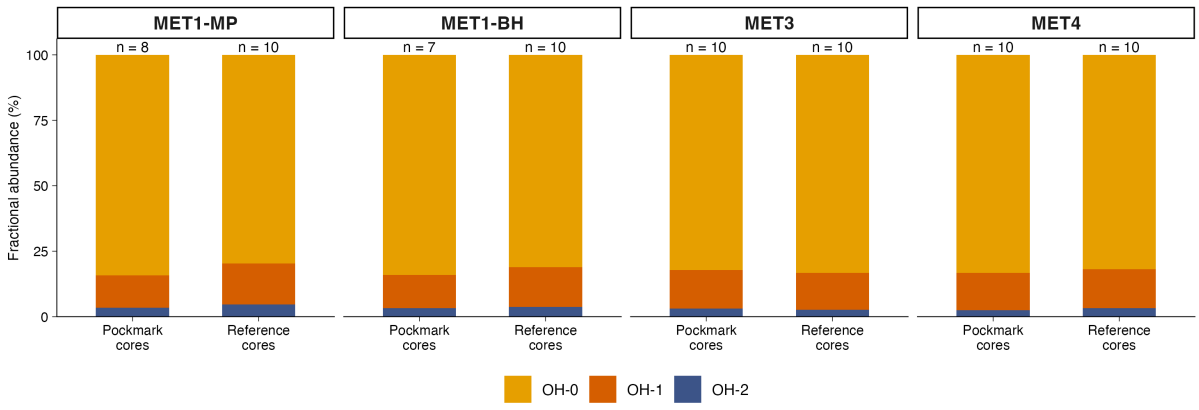

Fig. 9. Mean OH-GDGT fractional abundances in pockmark versus reference cores at sites MET1-MP, MET1-BH, MET3, and MET4 in the south-eastern Baltic Sea. Stacked bars show mean fractional

abundances of OH-0, OH-1 and OH-2, averaged by site and core type (pockmarks and references); n denotes the number of horizons (samples). OH-0 dominates across all sites, with OH-1 contributing a smaller yet consistent fraction and OH-2 occurring at low abundance.

3.5 Abundance and composition of archaea

Archaeal community composition differs between pockmark and reference sediments (Fig. 10). However, at the class level, most samples are dominated by Nanoarchaeia (Fig. 10a). Additional major contributions, at varying proportions, include Thermoplasmata, Methanosarcinia, Thermococci, Bathyarchaeia, Lokiarchaeia, and Methanomicrobia (Fig. 10a). Pockmark samples generally contain higher proportions of methane-cycling archaeal groups, particularly Methanosarcinia and Methanomicrobia, whereas reference cores more commonly show elevated contributions of Thermoplasmata, Bathyarchaeia, and Lokiarchaeia (Fig. 10a). The general depth trend shows Nanoarchaeia dominating shallower horizons, uniformly across reference and pockmark cores. Nanoarchaeia dominate the archaeal community in pockmarks, even in deeper sediment horizons, particularly at P/MET1-BH and P/MET1-MP. Vertical stratification is less consistent and more site-specific in pockmark cores than in reference cores, but the relative abundance of Methanosarcinia, Thermococci, and Bathyarchaeia increases downcore. Methanomicrobia also show a pockmark-associated pattern, with higher mean relative abundance in pockmarks than in references (2.6 ± 1.8% vs. 0.6 ± 1.0%, respectively), indicating additional methanogen-affiliated archaeal populations beyond Methanosarcinia (Fig. 10a). In reference cores, in deeper horizons, the community composition shifts towards a higher relative abundance of Thermoplasmata, Bathyarchaeia, Lokiarchaeia, and Deep Sea Euryarchaeotic Group (DSEG, currently within Thermoplasmatota; Rinke et al., 2021), suggesting a greater contribution from uncultivated anaerobic sedimentary archaeal lineages with depth. Across all samples, these classes were more abundant in reference than in pockmark cores, with mean relative abundances of 20.5 ± 13.6% vs. 9.4 ± 5.2% for Thermoplasmata, 14.8 ± 19.5% vs. 5.2 ± 5.9% for Bathyarchaeia, 5.6 ± 2.4% vs. 3.5 ± 2.6% for Lokiarchaeia, and 3.0 ± 1.7% vs. 2.0 ± 1.8% for DSEG.

Archaeoglobi were more abundant in reference sediments, averaging 1.7 ± 1.9% and 0.4 ± 0.6%, respectively, particularly in mid-depth horizons, where they may indicate a sulphur-cycling anaerobic archaeal community (Fig. 10a). Other low-abundance classes, including Micrarchaeia, Iainarchaeia, Altiarchaeia and Heimdallarchaeia, formed part of the archaeal rare

biosphere and exhibited localised enrichment in selected horizons. ANME-1 was detected only at trace relative abundance.

Nitrososphaeria were detected in both pockmark and reference cores, with taxonomic profiling revealing that this class is dominated almost exclusively by Nitrosopumilaceae (Fig. 10e, supplementary material Fig. S5) and, at the genus level, primarily by *Candidatus* Nitrosopumilus (Supplementary material Fig. S5a, b). Nitrosopumilaceae showed higher relative abundance in reference cores (14.0 ± 8.8%) than in pockmark cores (8.8 ± 3.7%), with maxima in deeper reference sediment strata. *Ca.* Nitrosopumilus was more abundant in reference cores, particularly in S/MET3/10, S/MET1-MP/10, and S/MET1-BH/10 (Supplementary material Fig. S5a, b). These distributional trends indicate that Nitrosopumilaceae-affiliated AOA are a more significant component of the biogeochemical nitrogen-cycling community in non-pockmark and deeper sediment horizons, whereas selected pockmark layers are comparatively enriched in archaeal taxa implicated in CH_4 cycling. This indicates that the distinction between pockmark and reference sediments is largely reflected in shifts in the relative abundance of CH_4-cycling, heterotrophic/fermentative, and ammonia-oxidising archaeal groups.

Hierarchical analysis at the class level showed four distinct clusters (Fig. 10b), with partial clustering of pockmark and reference samples and overlap between the pockmark and reference cores. Cluster 1 comprises the pockmark samples; Cluster 2 combines reference and pockmark samples; Cluster 3 groups mainly reference samples; and Cluster 4 comprises two S/MET1-BH reference samples and the P/MET4/10 sample (outliers). This pattern is consistent with the MDS ordination. The PERMANOVA test (Fig. 10c) indicates that the difference between pockmark and reference archaeal communities is statistically significant (p = 0.003). Multivariate analysis using MDS clearly shows clustering of samples into two categories – pockmarks vs references (Fig. 10c). However, some differences are noticeable: pockmark samples are more tightly clustered, whereas reference samples are slightly more dispersed. Based on the above analyses, it can be assumed that the pockmark cores differ significantly in their archaeal composition from the adjacent reference cores. Additionally, PCA analysis indicates the groups that may have the greatest impact on sample differentiation (Fig. 10d). For pockmarks, the greatest impact on sample variability is as follows: Hadarchaeia > Methanobacteria > Methanocellia > Halobacteria. In the reference samples, the order is Methanocellia > ANME-1 > Methanobacteria > Hadarchaeia. In both pockmark and reference

cores, the same groups contribute most to sample variability, although the proportions of these contributions differ; therefore, the compositions must differ.

Because several archaeal groups discussed in relation to methane cycling and ammonia oxidation are not resolved at the class level, the family-level heatmap is presented to clarify the distribution of key taxa (Fig. 10e). Additional figures in the supplementary material show extended family-level relative abundance profiles (Supplementary material Fig. S4), the genus-level heatmap with extended genus-level relative abundance profiles (Supplementary material Fig. S5a, b), and profiles revealing the relative abundances of methanogenic (Supplementary material Fig. S6) and methanotrophic (Supplementary material Fig. S7) archaeal groups.

At the family level, a few groups dominate both pockmark and reference cores, albeit in different proportions: SCGC_AAA011-D5, uncultured lineages, GW2011, and Nitrosopumilaceae (Fig. 10e). However, there are some site- and horizon-specific distinctions. Pockmark cores are characterised by a strong, localised enrichment of methane-cycling archaea, particularly ANME-2a/2b (mean relative abundance of 5.5 ± 9.3% vs 1.8 ± 3.1%), Methanosarcinaceae (5.0 ± 6.0% vs 3.4 ± 1.9%), Methanomicrobiaceae (2.2 ± 1.8% vs. 0.3 ± 0.4%), and Methanosaetaceae (1.8 ± 1.5% vs 0.8 ± 1.6%). These taxa show vertical heterogeneity, with relative abundances peaking at the middle and bottom of the profiles, i.e., ANME-2a/2b in the deeper parts of the pockmark cores (P/MET1-MP/7, P/MET4/10; Fig. 10e; Supplementary material Fig. S4), as well as Methanosarcinaceae (P/MET4/5; Fig. 10e; Supplementary material Fig. S4) and Methanomicrobiaceae (P/MET4/5; Fig. 10e; Supplementary material Fig. S4). Reference cores, by contrast, show a stronger contribution from Nitrosopumilaceae (14.0 ± 8.8% vs 8.8 ± 3.7%), Archaeoglobaceae (2.0 ± 2.3% vs. 0.5 ± 0.7%), Hadarchaeales (1.3 ± 2.0% vs 0.5 ± 0.7%), and uncultured lineages (25.3 ± 21.1% vs. 10.1 ± 7.4%) (Fig. 10e; supplementary material Fig. S4), which are characterised by variable depth-related trends.

At the genus level, both pockmark and reference cores are dominated by AR15, *Ca.* Nitrosopumilus, Methanosarcina, and AR20 (Supplementary material Fig. S5). However, the archaeal community in pockmark cores shows a higher relative contribution of methanotrophic taxa than in reference cores, i.e., ANME-3 (minor component; 0.7 ± 1.0% vs 0.1 ± 0.4%), particularly in cores P/MET1-BH and P/MET4, and ANME-2b (7.5 ± 12.3% vs 1.9 ± 4.1%), particularly in the upper and lower parts of the profiles P/MET1-MP and P/MET4; as well as

enrichment of methanogens, particularly at mid-depth in P/MET4: Methanosarcina (29.3%), Methanosaeta (8.2%), and Methanogenium (5.9%). In contrast, reference cores show a stronger representation of *Ca*. Nitrosopumilus (34.1 ± 17.7% vs. 22.3 ± 7.4%), particularly at mid-depth in S/MET3, as well as AR20 (7.5 ± 6.1% vs. 2.4 ± 1.8%) and Methanoregula (3.3 ± 6.1% vs. 2.8 ± 3.5%), particularly at the bottom of the S/MET1-BH profile.

The methanogenic and methanotrophic groups are not restricted to pockmarks; in the reference cores, their relative abundances are lower, yet they remain common. The summed relative abundance of methanotrophic archaeal groups is approximately fourfold higher in pockmark cores than in adjacent reference cores, averaging 8.3 ± 12.2% and 2.0 ± 4.1%, respectively. AOM-associated archaea, primarily ANME-2b and, to a lesser extent, ANME-3, are, however, enriched in selected pockmark horizons. Methanogenic archaea are abundant in both pockmark and reference cores, with a moderately higher average summed relative abundance in pockmarks (18 ± 11.4%) than in references (14.0 ± 11.4%). However, in pockmark cores, the diversity of methanogenic taxa, and to a lesser extent methanotrophic taxa, is higher (Supplementary material Figs. S6 and S7).

Archaeal read abundances were generally higher in pockmark cores than in reference cores, particularly at MET4, where abundances peak in the shallow horizon (Supplementary material Fig. S8). In pockmark cores, archaeal abundances typically peak in the upper to middle parts of the sampled profiles, except in P/MET1-BH, where the trend is reversed (Supplementary material Fig. S8). Similarly, in the reference cores, archaeal abundances peak in the upper to middle horizons, except in the S/MET1-BH core, where abundance increases with depth (Supplementary material Fig. S8).

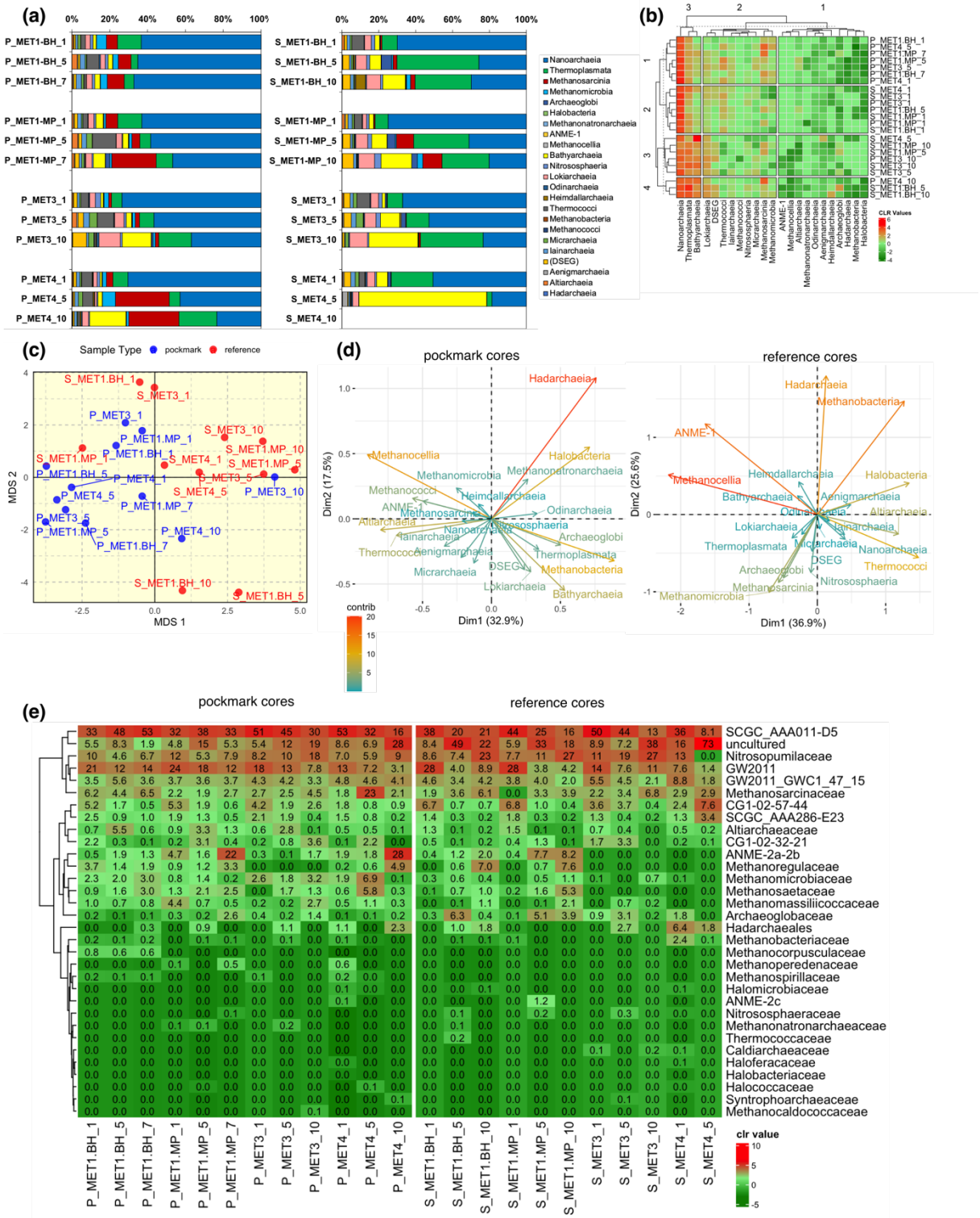

Fig. 10. Archaeal community composition and multivariate structure in pockmark and reference sediment cores from the south-eastern Baltic Sea. (a) Class-level relative abundance profiles (stacked bars) of archaeal communities in pockmark (P) and reference (S) sediment samples from MET1-BH, MET1-MP, MET3, and MET4. Bars show the proportional contribution of archaeal classes in each sample; sample suffixes indicate depth horizons (as explained in section 2.2). (b) Class-level heatmap of centred log-ratio (CLR)-transformed relative abundances, with hierarchical clustering (dendrograms)

of samples and archaeal classes, showing covariation among classes and samples, where red indicates higher relative enrichment and green indicates lower relative enrichment. (c) Multidimensional scaling (MDS) ordination of archaeal community composition shows partial separation between pockmark and reference samples (PERMANOVA, $p = 0.003$). NMDS shows significant separation (PERMANOVA, $p = 0.003$), with reference samples more dispersed and pockmark samples more tightly grouped. Taxa driving within-group variability differ between habitats: Hadarchaeia and Halobacteria dominate the pockmark ordination, whereas Methanobacteria, ANME and Hadarchaeia drive the reference ordination. (d) Ordination biplot showing the archaeal classes that contribute most strongly to community variation in pockmark and reference samples, respectively. Nanoarchaeia dominate across all sites. Pockmark horizons show elevated Methanosarcinia (MET1-MP, MET4), whereas reference horizons show stronger contributions from Thermoplasmata and/or Bathyarchaeia. Hierarchical clustering reveals partial intermixing of pockmark and reference samples, indicating that community structure reflects both habitat type and site-specific variability. (e) Family-level heatmap of archaeal relative abundance (CLR-transformed community structure), showing taxonomic groups not visible at the class level, including ANME-2a/2b.

3.6 Correlation network

To link GDGT patterns to probable biological sources, we combined iGDGT and OH-GDGT abundances with archaeal 16S rRNA relative abundances at the family level using correlation network analysis. This approach identified co-varying lipid–taxon modules that may indicate common sources, ecological niches, or interconnected processes rather than direct biosynthesis alone.

In pockmark sediments, the correlation network resolves three main archaeal communities that co-vary (Fig. 11). The first community (red) comprises the full suite of measured GDGTs and is most strongly connected to several Nanoarchaeia lineages (GW2011, SCGC_AAA286_E23, CG1.02.57.44, SCGC_AAA011.D5), with additional links to Methanoperedenaceae. The second community is dominated by ammonia-oxidising Nitrosopumilaceae and clusters with Hadarcheales. Within this module, Nitrosopumilaceae show the strongest positive associations with GDGT-0, the remaining iGDGTs, and OH-GDGTs. The same module contains ANME-2a/2b, Methanoregulaceae, and uncultured lineages that are strongly interconnected with one another but show comparatively weaker links to GDGTs. Archaeoglobaceae forms a peripheral node and does not meet the edge-retention criteria; no GDGTs were detected in pockmarks. The third community comprises methanogenic lineages, including *Methanospirill*aceae,

Methanobacteriaceae, Methanosarcinaceae, Methanosaetaceae, Methanomicrobiaceae, Methanomassiliicoccaceae and CG1.02.32.21 (associated with the order Micrarchaeales). These are less directly linked to GDGTs but strongly interlinked with one another. This cluster also includes another representative of Nanoarchaeia (GW2011_GWC1_47_15).

In reference sediments, GDGT associations are more broadly distributed across archaeal groups, and the network exhibits higher modularity, with clearer separation among modules. A lipid cluster (crenarchaeol, cren', GDGT-0-3, and OH-GDGTs) correlates with both ammonia oxidisers (Nitrosopumilaceae, Nitrososphaeraceae) and multiple methanogenic families (Methanosaetaceae, Methanosarcinaceae, Methanoregulaceae, Methanomicrobiaceae, Methanomassiliicoccaceae). Compared with pockmarks, methanogens show fewer direct links to the GDGT cluster and more to ANME-2a/2b. Archaeoglobaceae remains peripheral, with weak links to Nitrososphaeraceae and methanogens.

Overall, the pockmark network exhibits low modularity and relatively dense connectivity, indicating a closely coupled archaeal community. At the same time, the strongest GDGT links centre on Nitrosopumilaceae, implying that AOA dominate GDGT co-variation in these methane-rich sediments, whereas methanogens/ANME form more distinct sub-clusters with weaker GDGT coupling.

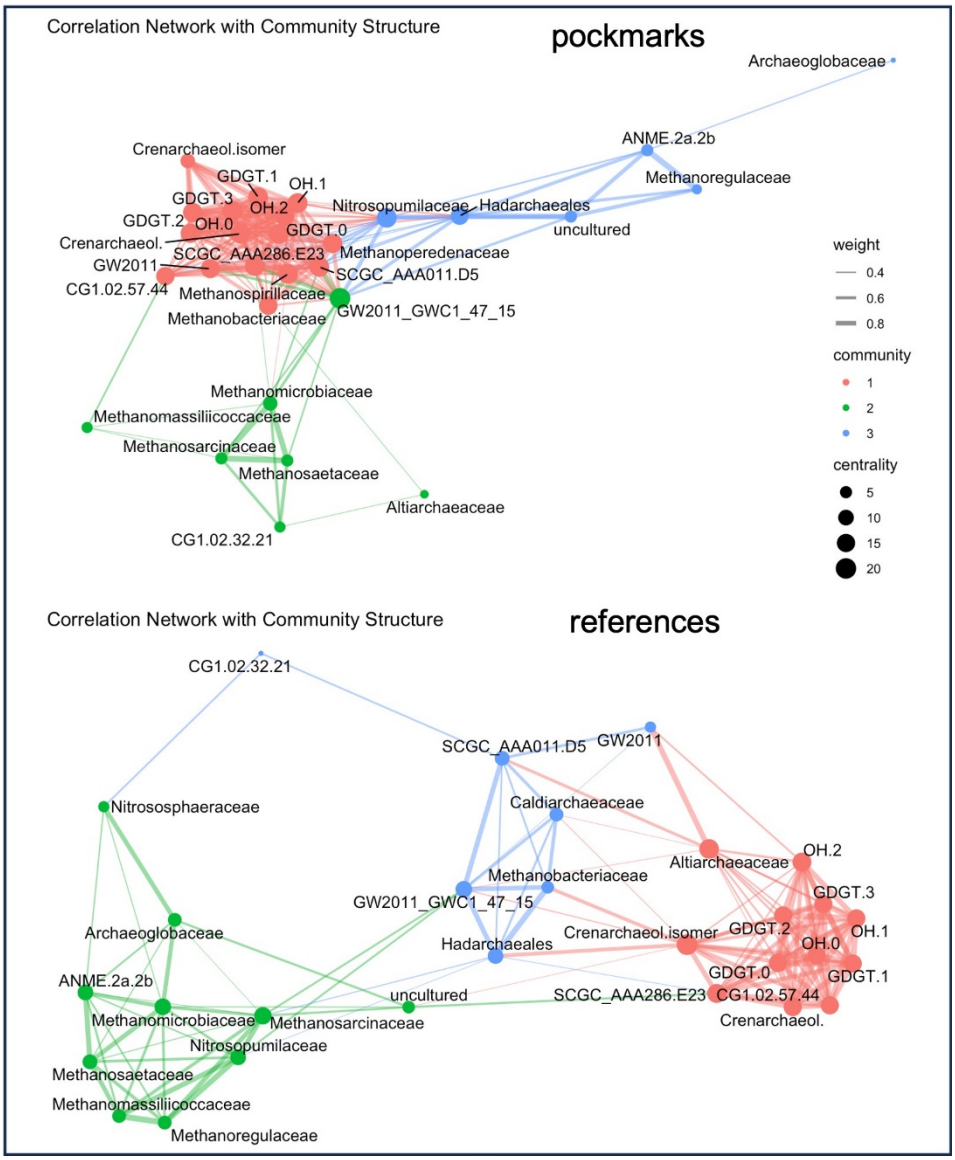

Fig. 11. Correlation networks linking archaeal lipid biomarkers and community members in pockmark and reference (non-pockmark) sediments. Nodes represent lipid variables (GDGTs, OH-GDGTs) and archaeal taxa (family level). Edge thickness reflects correlation strength; node colour denotes modules/communities (1–3); node size reflects centrality (larger nodes indicate more central or highly connected features). Lipid variables form a tightly connected subnetwork (module 1; red), while additional modules comprise methane-cycling and other archaeal lineages. Module connectivity differs between pockmark and non-pockmark sites, indicating habitat-dependent coupling between biomarkers and archaeal taxa. Pockmark networks show tighter coupling between lipid biomarkers and methane-cycling lineages, whereas reference sediments display clearer module separation, with lipids and the archaeal community varying more independently.

4 Discussion

4.1 Archaeal community structure in methane-influenced pockmark sediment cores

The archaeal community structure and porewater profiles of CH_4 and SO_4^{2-} indicate that the investigated pockmarks are CH_4-influenced yet spatially heterogeneous sedimentary systems. At the microbial community level, pockmark cores are not characterised by a complete replacement of the reference archaeal groups, but rather by localised enrichment of CH_4-cycling lineages. This is most clearly evident at lower taxonomic levels, where ANME-2a-2b/ANME-2b, Methanosarcinaceae, Methanosaetaceae, Methanomicrobiaceae, and other CH_4-associated taxa are enriched in selected pockmark horizons (Fig. 10e; supplementary material Figs. S4 and S5). Pockmark cores exhibit substantially higher methanogen diversity (11 genera detected) and a higher abundance of CH_4-cycling archaea (approximately threefold) than reference cores (6 genera) (Supplementary materials, Fig. S5a, b). Correspondingly, total iGDGT and OH-GDGT concentrations are approximately three times higher in pockmark cores than in reference cores (Fig. 6, 8). In the correlation network (Fig. 11), pockmarks represent a tightly coupled metabolic system in which various archaeal groups act in concert — likely CH_4-impacted — whereas at the reference sites these groups form less integrated sub-communities, with stronger representation of ammonia-oxidising *Ca*. Nitrosopumilus (Supplementary material Fig. S5a, b), heterotrophic Thermoplasmata associated with acidic, sulphur-rich environments (González-Toril et al., 2006), and organic matter-degrading Bathyarchaeia (Zhou et al., 2018). This suggests that in reference cores, microorganisms have more independent ecological roles, which could be explained by higher sulphate concentration and lower methane concentration (Fig. 2). On the other hand, the summed relative abundances of methanotrophic archaea are approximately fourfold higher in pockmark cores than in reference cores, whereas methanogens are moderately more abundant in pockmark cores than in reference cores. This suggests that AOM-associated lineages are more closely linked to pockmark niches, whereas methanogenic taxa occupy broader anoxic sedimentary niches. However, the Baltic Sea exhibits considerable microbial diversity due to eutrophication and pollution, steep horizontal and vertical gradients in salinity and nutrient levels, and the presence of freshwater and marine phyla, as well as autochthonous brackish populations (Ininbergs et al., 2015).

4.2 Methanogenic archaea and depth-related community shifts

Methanosarcina predominates across all sediment horizons in both pockmark and reference cores (Supplementary material Fig. S6), likely owing to its metabolic versatility (Sowers et al., 1993; Galagan et al., 2002; Maeder et al., 2006), which confers competitive advantages under fluctuating environmental conditions (e.g., hydrostatic pressure governing freshened porewater seepage, seasonal thermocline dynamics, nutrient availability, and North Sea saline water inflow). The vertical distribution of methanogenic archaea varies with sediment depth (Supplementary material, Fig. S6), whereas *Methanosarcina* and *Methanosaeta* predominantly populate the examined sediment horizons, except in the reference cores S/MET3 and S/MET4. Both taxa drive acetoclastic methanogenesis (Conklin et al., 2006; Welte et al., 2014) and are favoured in sediments rich in labile organic matter (Li et al., 2022). Both *Methanosarcina* and *Methanosaeta* are major contributors to the GDGT-0 pool in estuarine sediments (De Rosa et al., 1977; Schouten et al., 2013; Bauersachs et al., 2015). GDGT-0 is the second most abundant GDGT in the analysed samples (Fig. 7). The remaining major component of the methanogenic community that appears to alternate – sometimes with *Methanosaeta*, sometimes with SDB – is *Methanoregula* and *Methanogenium*, exhibiting a downcore shift.

Interestingly, *Methanosaeta* completely disappears in reference cores S/MET3 and S/MET4, being replaced by *Methanosarcinia*. In pockmark cores, *Methanosaeta* abundance declines remarkably in P/MET3 (especially in the uppermost sediment horizon) and in P/MET4 (especially in the lowermost horizon) and is replaced by diverse hydrogenotrophic genera, including *Methanospirillum, Methanogenium*, *Methanomicrobium, Methanoculleus, Methanocorpusculum, Methanobrevibacter,* and *Methanolinea*. Pockmark core P/MET4, which is characterised by the highest total GDGT concentrations and the most pronounced individual GDGT peaks (Fig. 6; supplementary material Fig. S2), alongside *Methanosarcina,* harbours exceptionally abundant hydrogenotrophic methanogens (particularly *Methanoregula*); pockmark core P/MET3 shows the next highest abundance. Microbial activity hotspots form at interfaces and in mixing zones (Stegen et al., 2016). This methanogenic community shift coincides with elevated CH_4 concentrations in the pockmarks P/MET3 and P/MET4 (Fig. 2). The hydrogenotrophs listed above belong to the class Methanomicrobia and are known to produce acyclic GDGT (Bale et al., 2019; Zeng et al., 2022). A genus such as *Methanobrevibacter* has been identified as a producer of GDGT-0 (Bauersachs et al., 2015; Elling et al., 2017). Similar hydrogenotrophic communities have been documented in an inactive pockmark within the Hanko Basin, northern Baltic Sea (Purkamo et al., 2022). In this dataset, pockmark P/MET3 was inactive during the study period and did not demonstrate

929 porewater freshening (Supplementary material Table S1), and pockmark P/MET4 is
930 characterised by weak activity.

931 **4.3 Porewater geochemistry, SMTZ development**

932 Porewater profiles of CH_4 and SO_4^{2-} show stronger CH_4 accumulation and sharper SO_4^{2-}
933 depletion, particularly at MET1-MP, MET1-BH, and MET4, indicating active or recent
934 methane supply and shallow-to-subsurface transition zones (from 5 to ~25 cm bsf) where CH_4
935 and SO_4^{2-} gradients overlap. In MET4, the strongest porewater methane enrichment coincides
936 with high relative abundance of Methanosarcinaceae/Methanosarcina at 40-45 cm bsf and with
937 high relative abundance of ANME-2a/2b/ANME-2b at 90-95 cm bsf (Fig. 10e; supplementary
938 material Figs. S4, S5a, b). MET1-MP also shows pronounced enrichment of ANME-
939 2a/2b/ANME-2b at 60-65 cm bsf (Fig. 10e; supplementary material Figs. S4, S5a, b), consistent
940 with the presence of methane below the shallow SMTZ. However, the microbial maxima do
941 not always coincide with the visually estimated SMTZ intervals, as expected, because the
942 porewater profiles represent a 'snapshot' of geochemical gradients at that time, whereas DNA-
943 based community structure may integrate temporal variability.

944 The interpretation is consistent with previous observations of Baltic pockmark sediments
945 reported by Iasakov et al. (2022), in which ANME lineages showed vertical niche separation:
946 ANME-2a/2b were predominant in upper horizons within the SMTZ, which in the Gdańsk Deep
947 region typically occurs between 20 and 40 cm bsf, whereas ANME-1a/1b were found in deeper
948 SO_4^{2-}-depleted sediments below the SMTZ, up to 280 cm bsf. In the samples studied, ANME-
949 1 occurs only at trace levels, suggesting that the sampled intervals primarily capture shallow-
950 to intermediate-depth CH_4-affected horizons. Therefore, the combined biomarker, porewater,
951 and microbiological data indicate a mosaic of CH_4-cycling niches, in which S-AOM,
952 methanogenesis, and porewater freshening govern complex redox zonation and mixed archaeal
953 lipid sources.

954 **4.4 Controls on archaeal lipid accumulation: methane cycling, LOI, and pockmark**
955 **activity**

956 The iGDGT distribution profiles offer an additional lipid-based perspective on the spatial
957 heterogeneity of the investigated pockmark systems. pockmark cores, particularly P/MET3 and
958 P/MET4, show elevated concentrations of archaeal lipids ∑iGDGT and ∑OH-GDGT (Figs. 6,

8) relative to adjacent reference cores, indicating enhanced archaeal lipid accumulation in selected pockmark cores. In the pockmark core P/MET4, high iGDGT concentrations coincide with strong porewater CH_4 enrichment, SO_4^{2-} depletion (Fig. 2), lower Cl^- concentrations relative to the reference core (Fig. 3), and local enrichment of methane-cycling archaea (Fig. 10e), including ANME-2b, ANME-3, and methanogen-affiliated genera (Supplementary material Figs. S5a, b, S6, S7). Taken together, these suggest that CH_4 cycling and possibly weak porewater freshening contributed to the archaeal lipid signal. The elevated GDGT-3 concentration in pockmark P/MET4 is also consistent with a locally increased contribution from ANME-3 (at P/MET4/5; supplementary material Fig. S5a), although GDGT-3 is not source-specific.

To assess whether elevated ∑iGDGT concentrations might simply reflect higher bulk organic matter content, GDGT profiles were compared with LOI-derived trends in organic matter (full-core elemental TOC data were not available for all sites) (Fig. 4). LOI was used as a screening-level proxy, supported by comparisons of measured TOC and LOI profiles in representative cores, which show comparable vertical trends (Fig. 4). This comparison indicates that ∑iGDGT and ∑OH-GDGT concentrations are not tightly coupled to bulk organic matter (Figs. 4-6, 8). In several cores, GDGT profiles do not align with LOI trends: for example, pockmark P/MET1-BH shows relatively high LOI and clear CH_4 enrichment with SO_4^{2-} depletion, yet does not exhibit the strongest GDGT accumulation, whereas pockmark P/MET3 contains elevated ∑iGDGT and ∑OH-GDGT concentrations despite weaker porewater CH_4 enrichment and a smaller contribution from methane-cycling archaea than P/MET4. Similarly, the strong GDGT enrichment cannot be explained by LOI alone, because the lipid maxima align more closely with steep CH_4/SO_4^{2-} gradients and with pockmark archaeal community abundance than with a simple increase in bulk organic matter. Additionally, the generally low BIT values indicate that terrestrial-derived brGDGT input is minor across the investigated sites. This suggests that the iGDGT pool is dominated by marine archaeal lipids. However, the deepest intervals of the S/MET4 reference core show slightly elevated BIT values, indicating a localised increase in the relative contribution of brGDGTs. BIT can also be affected by the decline in crenarchaeol. However, brGDGTs may also be produced in marine sediments (although their molecular composition differs) (Peterse et al., 2009; Sinninghe Damsté, 2016). Thus, elevated ∑GDGT concentrations cannot be attributed solely to increased TOC or bulk organic matter accumulation. Instead, they appear to reflect multiple, partially decoupled controls, including archaeal community composition and abundance, and the probable contributions of water-

column and sedimentary GDGT sources. Lipid preservation could also be a side effect of the less ebullitive nature of methane seepage in pockmarks P/MET3 and P/MET4: the kinetics and episodicity of CH_4 supply and freshened porewater discharge, which influence redox zonation. As reported by Treude et al. (2005) in Eckernförde Bay, the spatial and temporal heterogeneity caused by gas ebullition allows methanogens and sulphate reducers to coexist, feeding the shallow SMTZ, and also enables methane to escape into the overlying water column, bypassing the microbial barrier. This is particularly important for the more hydrologically complex pockmarks MET1-BH and MET1-MP with porewater freshening, where present-day dissolved CH_4 and SO_4^{2-} profiles may not fully capture the timing or intensity of CH_4 supply.

The partial mismatch among porewater chemistry, archaeal community composition, and GDGT concentrations therefore suggests that CH_4 cycling in these sediments cannot be described by a simple sulphate-controlled SMTZ model alone. P/MET1-BH, for instance, shows strong CH_4 enrichment and SO_4^{2-} depletion, indicating an active or recently active methane-influenced redox zone (Fig. 2). However, its GDGT concentrations are much lower than those in pockmarks P/MET3 and P/MET4. Conversely, P/MET3 shows substantial GDGT accumulation despite weaker porewater methane enrichment and a less pronounced archaeal presence involved in CH_4 cycling. This decoupling suggests that the bulk GDGT pool integrates *in situ* archaeal production, pelagic input of Nitrossopaheria-derived crenarchaeol, contributions from sedimentary lineages such as Thermoplasmata and other uncultivated archaea, and preservation effects.

4.5 Porewater freshening and potential alternative methane oxidation pathways

In addition, porewater freshening and CH_4 ebullition to the water column may modify the redox zone of the active pockmark sediments at stations P/MET1-BH and P/MET1-MP (Supplementary material Table S1). Chloride profiles, particularly in the MET1 area and MET4, show lower chloride concentrations in pockmark cores relative to adjacent reference cores (Fig. 3), indicating a potential influence of freshened porewater in diluting SO_4^{2-} and shifting the depth, intensity, and archaeal community structure of the methane oxidation zone. Although S-AOM is expected near the CH_4-SO_4^{2-} overlap, pockmarks P/MET1-BH and P/MET1-MP, affected by freshened groundwater seepage, may also host deeper CH_4 oxidation zones, where electron acceptors other than SO_4^{2-} could become more relevant.

Kurowski et al. (2024) concluded that Fe-AOM may occur in MET1-BH sediments. Additionally, it was suggested that freshened groundwater seepage dilutes the already low chloride and sulphate concentrations in the pockmarks MET1-BH and MET1-MP (Brodecka-Goluch et al., 2022; Idczak et al., 2020; Łukawska-Matuszewska and Dwornik, 2025). Water salinity inside the MET1-BH pockmark crater was measured at ~2 PSU, with Cl^- concentrations 93% lower than in typical marine porewater in the region. Fluctuating low-oxygen to anoxic conditions in the bottom waters of the MET1 area, promoting steep redox gradients (sharply decreasing SO_4^{2-} concentrations) that favour methanogenesis; these conditions, further enhanced by anthropogenic contamination, create conditions for intensive organic matter mineralisation, were also reported (Idczak et al., 2020; Brodecka-Goluch et al., 2022). Furthermore, Purkamo et al. (2022) showed that SGD-driven advection in northern Baltic Sea pockmarks can compress redox and reaction zones to the uppermost centimetres, reduce organic matter accumulation, and suppress SMTZ development. In such active pockmarks, archaeal communities are dominated by AOA (Purkamo et al., 2022). Conversely, inactive pockmarks dominated by diffusion accumulate organic-rich, fine-grained sediments that are characterised by SO_4^{2-} reduction and methanogenesis, with methanogens prominent within the archaeal community.

4.6 Evaluation of GDGT-based methane proxies in Gdańsk Basin pockmarks

4.6.1 Limitations of GDGT-based AOM proxies in ANME-2/ANME-3-dominated pockmarks

Peaks in archaeal abundance (Supplementary material Fig. S8) and in GDGT concentrations at sediment depths of 5–45 cm could mark the SMTZ (Fig. 2). However, iGDGTs indices (Table 1) do not support a strong AOM imprint, as values remain uniformly low. MI values (<0.09) fall well below the 0.3-0.5 threshold indicative of CH_4-impacted sediments observed by Zhang et al. (2011). However, for the MI value to reach 0.5, methanotrophic-derived GDGT must constitute approximately 30-50% of the total GDGT pool (Kim and Zhang, 2023).

A low MI index, calculated as the ratio of GDGT-1-3 to crenarchaeol, typically indicates minimal methanotrophic contribution relative to Nitrososphaeria-derived sources (Zhang et al., 2011). The uniformly low MI values observed here likely reflect a strong crenarchaeol signal from ammonia-oxidising archaea thriving above, in the water column and/or limited GDGT-1-3 production by the dominant AOM lineages, rather than definitively excluding AOM. GDGT-1 to -3, which increase substantially in ANME-1-dominated systems (Rossel et al., 2008), are

two orders of magnitude less abundant in the analysed samples than GDGT-0 and crenarchaeol, consistent with the near-absence of ANME-1 (maximum relative abundance of 0.6% in S/MET3/5; Fig. 10a).

Although the applicability of MI to ANME-2 and ANME-3 (which dominate the AOM community here; supplementary material Fig. S7) has been questioned, comprehensive biomarker investigations generally support its utility for AOM detection (Kim and Zhang, 2023). Nevertheless, ANME-2 and ANME-3 alone are unlikely to contribute substantially to GDGT production (Niemann and Elvert, 2008; Weijers et al., 2011), making MI non-diagnostic in this study. The consistently low GDGT-2/cren ratios (maximum 0.04; Table 1) support this interpretation. This ratio typically indicates CH_4-rich AOM conditions, under which ANME-1-synthesised GDGT-2 (Rossel et al., 2008) is elevated relative to crenarchaeol. To further evaluate the GDGT distribution characteristics of an AOM-related SMTZ, the relative abundances of GDGT-1, GDGT-2, and GDGT-3 were compared across cores. In contrast to the GDGT-2-dominated pattern reported by Weijers et al. (2011), GDGT-2 was not the dominant compound in any of our samples. Instead, 74 of 75 samples showed the order GDGT-1 > GDGT-2 > GDGT-3. This indicates that the investigated cores do not show enrichment of GDGT-2, consistent with uniformly low GDGT-2/crenarchaeol ratios.

Nevertheless, ANME lineages are more prevalent in pockmark cores (Supplementary material Fig. S7), suggesting, relatively to reference cores, enhanced AOM activity, particularly at P/MET3 and P/MET4. Peaks in GDGT-1 to -3 concentrations also occur in reference cores, following the general trend for all iGDGTs but at lower concentrations (Supplementary material Fig. S2). In addition, certain core GDGTs (e.g., GDGT-1) may arise from diagenetic and degradative processes acting on phosphohexose headgroups predominantly produced by *Ca.* Nitrosopumilus in the Baltic Sea (Wittenborn et al., 2023).

Overall, AOM activity appears constrained within the studied pockmarks, consistent with previous investigations demonstrating weak S-AOM confined to thin, shallow sediment layers and potentially dependent on alternative electron acceptors in deeper layers (Brocławik et al., 2020; Idczak et al., 2020; Brodecka-Goluch et al., 2022; Łukawska-Matuszewska et al., 2022; Ehlert von Ahn et al., 2024). The minor contribution of *Ca.* Methanoperedens in the dataset (MET1-MP; supplementary material Fig. S7) indicates traces of AOM coupled to nitrate and/or metal oxide reduction. Members of the family Methanoperedenaceae (formerly ANME-2D) typically inhabit sulphate-depleted freshwater systems and perform AOM independently of

syntrophic partnerships (Haroon et al., 2013; Ettwig et al., 2016; Vaksmaa et al., 2017; Leu et al., 2020).

4.6.2 Methanogens and GDGT-based proxies

Within the CH_4-cycling archaeal community, methanogens appear to be the primary contributors to GDGT biosynthesis (Fig. 7). Although GDGT-0 and crenarchaeol predominate in marine sediments (Schouten et al., 2002), their elevated concentrations across all investigated gas systems indicate that they serve as primary iGDGT biomarkers in the sediments of the Gdańsk Basin, even in CH_4-rich settings harbouring both methanogenic and methanotrophic communities. However, GDGT-0 lacks source specificity and can be synthesised by multiple archaeal lineages, including methanogens and methanotrophs (Pancost et al., 2001; Blaga et al., 2009; Inglis et al., 2015; Słowakiewicz et al., 2016; Petrick et al., 2019). These lineages may also produce cyclised GDGTs (Koga et al., 1993; Weijers et al., 2006; Schouten et al., 2013; Bauersachs et al., 2015), although this is not always replicable in culture studies (Bauersachs et al., 2015).

The network analysis indicates that AOA-associated crenarchaeol and the statistically co-varying GDGT-0 are the primary drivers of variation in the bulk GDGT pool (Fig. 11), likely masking the methanogen signal by influencing the GDGT-0/cren ratio through pelagic Nitrososphaerota contribution. The observed GDGT-0/cren ratios in Gdańsk Basin samples are <0.99, well below the 2 threshold characteristic of methanogen-dominated systems (Schouten et al., 2002; Blaga et al., 2009), indicating minimal methanogen contribution and AOA predominance. In the northern Baltic Sea pockmarks (Hanko Basin), Nitrososphaeria – including some groundwater-origin populations – constitute a major component of the archaeal community (Purkamo et al., 2022), consistent with evidence that *Ca*. Nitrosopumilus is widespread in the Baltic Sea and is an important GDGT-producing lineage (Wittenborn et al., 2023). However, amplicon-based relative abundance reflects the compositional distribution of recovered 16S rRNA gene reads after DNA extraction (Gloor et al., 2017) and does not directly indicate lipid production rates. By contrast, sedimentary iGDGTs integrate archaeal lipid production and export over longer timescales, and their distribution is further shaped by preservation conditions (Lengger et al., 2013).

4.7 AOA and non-methane archaeal lipid sources

Given that AOA are abundant in the Baltic Sea under low-oxygen conditions and along redox gradients (Berg et al., 2015b), the consistently low GDGT-0/cren ratios (<1) observed herein indicate a crenarchaeol-rich iGDGT pool, suggesting a substantial pelagic contribution from the settling and export of AOA-derived crenarchaeol from the water column. Methane seepage creates chemically reducing conditions that limit the growth of oxygen-dependent organisms. However, seep systems also generate sharp chemical gradients and microenvironments (e.g., thin oxic/suboxic boundary layers) in which AOA can persist and function (Jakobs et al., 2016). Martens-Habbena and Qin (2022) showed that *Nitrosopumilus maritimus* can sustain ammonia oxidation under oxygen-depleted conditions, further indicating that AOA may be flexible and physiologically adapted to redox-variable conditions. Nevertheless, elevated summed iGDGT and OH-GDGT concentrations in pockmarks MET3 and MET4 (especially GDGT-0 and crenarchaeol) may indicate an indirect ecological linkage between the nitrogen and carbon biogeochemical cycles in the studied system, in which degradation of organic matter, methanogenesis, sulphate reduction, and other anaerobic processes release NH_4^+ and other reduced compounds into porewaters. These compounds may subsequently be transported (diffused) into the bottom waters and the overlying water column, where Nitrososphaeria thrive. Consequently, crenarchaeol remains the dominant iGDGT in both pockmark and reference cores (Supplementary material Fig. S2), as Nitrososphaeria is abundant in the overlying water column and may feed on the products of enhanced processes occurring in the sediments. Despite this AOA dominance, GDGT-0 concentrations remain relatively elevated across the pockmark sites, particularly at the inactive pockmark MET3 and the weakly active pockmark MET4, which experiences weak, occasional porewater seepage, compared with active venting systems characterised by advective methane flow, such as mud volcanoes on the Canadian Beaufort Sea slope (Lee et al., 2018) and studied here pockmarks MET1-MP and MET1-BH (Supplementary material Fig. S2).

Average OH-GDGT% values align with those reported for Baltic Sea surface sediments (Sinninghe Damsté et al., 2022), and RI-OH and RI-OH values are within the Baltic/Skagerrak Surface sediment ranges (Sinninghe Damsté et al., 2022). While salinity primarily controls OH-GDGT behaviour (Sinninghe Damsté et al., 2022), recent studies show strong responses to nitrate availability and water-column stratification (Harning and Sepúlveda, 2024), indicating an ecological influence on RI-OH/RI-OH′. The most robust interpretation is that OH-GDGTs primarily track AOA, particularly Nitrososphaeria, as supported by culture studies (Sinninghe

Damsté et al., 2022). In our data, OH-GDGTs closely covary with crenarchaeol, consistent with previous findings indicating thaumarchaeal source (Kaiser and Arz, 2016).

Nanoarchaeota, prevalent across the samples, may be involved in ectosymbiosis with Nitrososphaeria, consistent with their reliance on symbiotic relationships (Waters et al., 2003). Nanoarchaeota may also possess GDGTs, previously attributed to their biological hosts (Zeng et al., 2022), which could explain their correlation with GDGTs (Fig. 6). They can also associate with methanogens (Brick et al., 2025), which may explain their high relative abundance (~40% in non-pockmark and ~55% in pockmark sediments). Other frequent groups (e.g., AR15, AR20) are likewise symbiotic or parasitic; the latter, linked to groundwater (Castelle et al., 2015), underscores the influence of porewater freshening in the Gulf of Gdańsk in pockmarks MET1-MP and MET1-BH.

Several archaeal groups, including Thermoplasmata, Bathyarchaeia, Lokiarchaeia, Heimdallarchaeia, Archaeoglobi, and the Deep Sea Euryarchaeotic Group (DSEG; within Thermoplasmatota; Rinke et al., 2021), are associated with the degradation of complex organic matter, aromatic carbon degradation, protein catabolism, and fermentation (Zinke et al., 2019). These groups — particularly Bathyarchaeia and Thermoplasmata — are more abundant in reference cores than in pockmarks and may contribute to GDGT production in anoxic environments (Besseling et al., 2018, 2020; Baxter et al., 2021). Bathyarchaeia thrive in anoxic environments, degrading recalcitrant organic matter (Baxter and Zalar, 2019; Blewett et al., 2022; Zeng et al., 2022), whereas Archaeoglobi mediate both sulphate reduction and methanogenesis (Lynes et al., 2024). Bathyarchaeia may also occupy a central position in archaeal carbon-nitrogen networks, co-occurring with methanogens and Nitrososphaeria, and potentially linking organic carbon degradation with reduced nitrogen availability (Yi et al., 2024). However, despite the abundance of Bathyarchaeia and Nitrososphaeria in the archaeal community structure, this mechanism remains inferential, as NH_4^+ and AOA activity were not directly measured herein. Asgard archaea, including hydrocarbon-degrading Lokiarchaeia and hydrogen-dependent acetogenic Heimdallarchaeia (Zhang et al., 2025), also show higher abundance in reference cores and may contribute to iGDGT production, likely GDGT-0 (Zeng et al., 2022). Although the tetraether synthase (Tes) gene, essential for GDGT biosynthesis, has been identified in Hadarchaeia and Altiarchaeia, GDGTs have not yet been detected in these groups (Zeng et al., 2022). Notably, some Hadarchaeia grow syntrophically with methanogens (Yu et al., 2024).

5. Conclusions

This study presents the first integrated analysis of archaeal 16S rRNA communities, sedimentary iGDGT/OH-GDGT distributions, and microbial correlation networks in methane pockmarks of the Gdańsk Basin. Pockmarks host more diverse and abundant archaeal communities than adjacent reference sites and function as tightly coupled metabolic systems, whereas reference sites exhibit more niche-partitioned ecological structures. Despite CH_4-rich conditions, evidence for anaerobic oxidation of methane (AOM) remains limited. Low MI values and the near absence of ANME-1 reduce the reliability of GDGT-based AOM proxies in settings with low ANME-1 abundance. Low GDGT-0/cren and GDGT-2/cren ratios indicate dominance of pelagic AOA, particularly *Ca*. Nitrosopumilus, which may mask methanogenic GDGT signals. However, the dominance of GDGT-0 and crenarchaeol within specific pockmarks may reveal intricate linkages between microbial community structure, i.e., Bathyarchaeia and Nitrososphaeria, and the underlying biogeochemical processes. The transport of reduced compounds from anaerobic reactions across the sediment-water interface may enhance the proliferation of Nitrososphaeria.

Results suggest that porewater freshening and pockmark activity, including gas ebullition, strongly influence geochemical conditions and archaeal distributions. The mixing of freshened groundwater with marine porewater, together with gas seepage, may create localised microbial "hotspots" with higher archaeal diversity. Differences between active (P/MET1) and inactive (P/MET3) or weakly active (P/MET4) pockmarks are reflected in archaeal community structure and GDGT concentrations. Methane cycling appears highly localised rather than continuous downcore. The clearest combined microbiological and biomarker evidence for methane cycling is observed at P/MET4, where elevated CH_4, SO_4^{2-} depletion, increased iGDGT concentrations, enrichment of ANME-2b, ANME-3, hydrogenotrophic methanogens, *Methanosarcina*, and *Methanosaeta* co-occur. However, the iGDGT distribution in the weakly active pockmark P/MET4 probably indicates a pelagic AOA source. In contrast, active MET1 pockmarks show iGDGT distributions similar to those of adjacent reference cores. The inactive pockmark P/MET3 shows increased archaeal lipid accumulation, but, as in pockmark P/MET4, this accumulation is primarily associated with pelagic AOA rather than with CH_4-cycling communities.

Future studies should integrate GDGT analyses with methane-specific biomarkers (e.g., crocetane, PMI, archaeol, hydroxyarchaeol), NH_4^+ concentrations, compound-specific carbon

isotopes, and functional gene or transcriptomic approaches (e.g., *mcrA*) to better constrain active CH_4 cycling and identify the responsible ANME clades, as well as spatial activity of Nitrososphaeria. Measuring both core and intact polar lipids in sediments and the water column would further clarify GDGT production, transport, and preservation. Overall, this study highlights the need for integrated multi-proxy and multi-omic approaches to distinguish active microbial processes from preserved diagenetic signals in methane seep systems influenced by submarine groundwater discharge, porewater freshening, and dynamic redox conditions.

Data availability. All iGDGT data is available in the repository 10.5281/zenodo.18414700.

Author contributions. IDMS and MS designed the research; IDMS evaluated the geochemical and microbiological data; AB, ABG, and KLM collected the samples; AB prepared the microbiological dataset; IDMS and AB conducted the statistical analyses; IDMS wrote the manuscript; FP and MS reviewed and edited the manuscript.

Competing interests. The contact author has declared that none of the authors has any competing interests.

Acknowledgements. This study was partially funded by the Elsevier Research Scholarship (awarded to IDMS). IDMS is grateful to the Organic Geochemistry Group at Utrecht University for assistance with analyses. AB, ABG, and KLM thank the captain and crew of RV *Oceanograf* for their support during the cruises. Paweł Działak is thanked for isolating material for DNA analysis. We are also indebted to two anonymous reviewers for their detailed and helpful comments.

References

Aitchison, J.: The statistical analysis of compositional data, Journal of the Royal Statistical Society: Series B (Methodological), 44, 139–160, https://doi.org/10.1111/j.2517-6161.1982.tb01195.x, 1982.

Bale, N. J., Palatinszky, M., Rijpstra, W. I. C., Herbold, C. W., Wagner, M., and Sinninghe Damsté, J. S.: Membrane lipid composition of the moderately thermophilic ammonia-oxidizing archaeon "Candidatus Nitrosotenuis uzonensis" at different growth temperatures, Applied and Environmental Microbiology, 85, e01332-19, https://doi.org/10.1128/AEM.01332-19, 2019.

Bauersachs, T., Weidenbach, K., Schmitz, R. A., and Schwark, L.: Distribution of glycerol ether lipids in halophilic, methanogenic and hyperthermophilic archaea, Organic Geochemistry, 83–84, 101–108, https://doi.org/10.1016/j.orggeochem.2015.03.009, 2015.

Baxter, A. J., van Bree, L. G. J., Peterse, F., Hopmans, E. C., Villanueva, L., Verschuren, D., and Sinninghe Damsté, J. S.: Seasonal and multi-annual variation in the abundance of isoprenoid GDGT membrane lipids and their producers in the water column of a meromictic equatorial crater lake (Lake Chala, East Africa), Quaternary Science Reviews, 273, 107263, https://doi.org/10.1016/j.quascirev.2021.107263, 2021.

Baxter, B. K. and Zalar, P.: The extremophiles of Great Salt Lake: Complex microbiology in a dynamic hypersaline ecosystem, in: Model Ecosystems in Extreme Environments, edited by: Seckbach, J. and Rampelotto, P., Academic Press, 57–99, https://doi.org/10.1016/B978-0-12-812742-1.00004-0, 2019.

Berg, C., Listmann, L., Vandieken, V., Vogts, A., and Jürgens, K.: Chemoautotrophic growth of ammonia-oxidizing Thaumarchaeota enriched from a pelagic redox gradient in the Baltic Sea, Frontiers in Microbiology, 5, https://doi.org/10.3389/fmicb.2014.00786, 2015a.

Berg, C., Vandieken, V., Thamdrup, B., and Jürgens, K.: Significance of archaeal nitrification in hypoxic waters of the Baltic Sea, The ISME Journal, 9, 1319–1332, https://doi.org/10.1038/ismej.2014.218, 2015b.

Besseling, M. A., Hopmans, E. C., Boschman, R. C., Sinninghe Damsté, J. S., and Villanueva, L.: Benthic archaea as potential sources of tetraether membrane lipids in sediments across an oxygen minimum zone, Biogeosciences, 15, 4047–4064, https://doi.org/10.5194/bg-15-4047-2018, 2018.

Besseling, M. A., Hopmans, E. C., Bale, N. J., Schouten, S., Damsté, J. S. S., and Villanueva, L.: The absence of intact polar lipid-derived GDGTs in marine waters dominated by Marine Group II: Implications for lipid biosynthesis in Archaea, Scientific Reports, 10, 294, https://doi.org/10.1038/s41598-019-57035-0, 2020.

Bijl, P. K., Śliwińska, K. K., Duncan, B., Huguet, A., Naeher, S., Rattanasriampaipong, R., Sosa-Montes de Oca, C., Auderset, A., Berke, M. A., Kim, B. S., Davtian, N., Dunkley Jones, T., Eefting, D. D., Elling, F. J., Fenies, P., Inglis, G. N., O'Connor, L., Pancost, R. D., Peterse, F., Rice, A., Sluijs, A., Varma, D., Xiao, W., and Zhang, Y. G.: Reviews and syntheses: Best practices for the application of marine GDGTs as proxy for paleotemperatures: sampling, processing, analyses, interpretation, and archiving protocols, Biogeosciences, 22, 6465–6508, https://doi.org/10.5194/bg-22-6465-2025, 2025.

Blaga, C. I., Reichart, G.-J., Heiri, O., and Sinninghe Damsté, J. S.: Tetraether membrane lipid distributions in water-column particulate matter and sediments: a study of 47 European lakes along a north–south transect, Journal of Paleolimnology, 41, 523–540, https://doi.org/10.1007/s10933-008-9242-2, 2009.

Blainey, P. C., Mosier, A. C., Potanina, A., Francis, C. A., and Quake, S. R.: Genome of a low-salinity ammonia-oxidizing archaeon determined by single-cell and metagenomic analysis, PLoS One, 6, e16626, https://doi.org/10.1371/journal.pone.0016626, 2011.

Blewett, J., Elling, F. J., Naafs, B. D. A., Kattein, L., Evans, T. W., Lauretano, V., Gallego-Sala, A. V., Pancost, R. D., and Pearson, A.: Metabolic and ecological controls on the stable

carbon isotopic composition of archaeal (isoGDGT and BDGT) and bacterial (brGDGT) lipids in wetlands and lignites, Geochimica et Cosmochimica Acta, 320, 1–25, https://doi.org/10.1016/j.gca.2021.12.023, 2022.

Blondel, V. D., Guillaume, J.-L., Lambiotte, R., and Lefebvre, E.: Fast unfolding of communities in large networks, Journal of Statistical Mechanics: Theory and Experiment, 2008, P10008, https://doi.org/10.1088/1742-5468/2008/10/P10008, 2008.

Boetius, A., Ravenschlag, K., Schubert, C. J., Rickert, D., Widdel, F., Gieseke, A., Amann, R., Jørgensen, B. B., Witte, U., and Pfannkuche, O.: A marine microbial consortium apparently mediating anaerobic oxidation of methane, Nature, 407, 623–626, https://doi.org/10.1038/35036572, 2000.

van den Boogaart, K. G., Tolosana-Delgado, R., and Bren, M.: Package "compositions": Compositional Data Analysis, 2024.

Brick, S., Niggemann, J., Reckhardt, A., Könneke, M., and Engelen, B.: Interstitial microbial communities of coastal sediments are dominated by Nanoarchaeota, Frontiers in Microbiology, 16, 1532193, https://doi.org/10.3389/fmicb.2025.1532193, 2025.

Brocławik, O., Łukawska-Matuszewska, K., Brodecka-Goluch, A., and Bolałek, J.: Impact of methane occurrence on iron speciation in the sediments of the Gdansk Basin (Southern Baltic Sea), Science of The Total Environment, 721, 137718, https://doi.org/10.1016/j.scitotenv.2020.137718, 2020.

Brodecka, A., Majewski, P., Bolałek, J., and Klusek, Z.: Geochemical and acoustic evidence for the occurrence of methane in sediments of the Polish sector of the southern Baltic Sea*, Oceanologia, 55, 951–978, https://doi.org/10.5697/oc.55-4.951, 2013.

Brodecka-Goluch, A., Idczak, J., Gorska, N., and Bolałek, J.: Geophysical and geochemical characteristics of four different pockmark sites located in the Gdańsk Basin, in: Earth system changes and Baltic Sea coasts, 89–90, 2020.

Brodecka-Goluch, A., Łukawska-Matuszewska, K., Kotarba, M. J., Borkowski, A., Idczak, J., and Bolałek, J.: Biogeochemistry of three different shallow gas systems in continental shelf sediments of the South-Eastern Baltic Sea (Gulf of Gdańsk): Carbon cycling, origin of methane and microbial community composition, Chemical Geology, 597, 120799, https://doi.org/10.1016/j.chemgeo.2022.120799, 2022.

Burnett, W. C., Bokuniewicz, H., Huettel, M., Moore, W. S., and Taniguchi, M.: Groundwater and pore water inputs to the coastal zone, Biogeochemistry, 66, 3–33, https://doi.org/10.1023/B:BIOG.0000006066.21240.53, 2003.

Burnett, W. C., Aggarwal, P. K., Aureli, A., Bokuniewicz, H., Cable, J. E., Charette, M. A., Kontar, E., Krupa, S., Kulkarni, K. M., Loveless, A., Moore, W. S., Oberdorfer, J. A., Oliveira, J., Ozyurt, N., Povinec, P., Privitera, A. M. G., Rajar, R., Ramessur, R. T., Scholten, J., Stieglitz, T., Taniguchi, M., and Turner, J. V.: Quantifying submarine groundwater discharge in the coastal zone via multiple methods, Science of The Total Environment, 367, 498–543, https://doi.org/10.1016/j.scitotenv.2006.05.009, 2006.

Bussmann, I. and Suess, E.: Groundwater seepage in Eckernförde Bay (Western Baltic Sea): Effect on methane and salinity distribution of the water column, Continental Shelf Research, 18, 1795–1806, https://doi.org/10.1016/S0278-4343(98)00058-2, 1998.

Callow, B., Bull, J. M., Provenzano, G., Böttner, C., Birinci, H., Robinson, A. H., Henstock, T. J., Minshull, T. A., Bayrakci, G., Lichtschlag, A., Roche, B., Yilo, N., Gehrmann, R., Karstens, J., Falcon-Suarez, I. H., and Berndt, C.: Seismic chimney characterisation in the North Sea – Implications for pockmark formation and shallow gas migration, Marine and Petroleum Geology, 133, 105301, https://doi.org/10.1016/j.marpetgeo.2021.105301, 2021.

Carman, R. and Jonsson, P.: Distribution patterns of different forms of phosphorus in some surficial sediments of the Baltic Sea, Chemical Geology, 90, 91–106, https://doi.org/10.1016/0009-2541(91)90036-Q, 1991.

Castelle, C. J., Wrighton, K. C., Thomas, B. C., Hug, L. A., Brown, C. T., Wilkins, M. J., Frischkorn, K. R., Tringe, S. G., Singh, A., Markillie, L. M., Taylor, R. C., Williams, K. H., and Banfield, J. F.: Genomic expansion of domain Archaea highlights roles for organisms from new phyla in anaerobic carbon cycling, Current Biology, 25, 690–701, https://doi.org/10.1016/j.cub.2015.01.014, 2015.

Chen, S., Zhou, Y., Chen, Y., and Gu, J.: fastp: an ultra-fast all-in-one FASTQ preprocessor, Bioinformatics, 34, i884–i890, https://doi.org/10.1093/bioinformatics/bty560, 2018.

Conklin, A., Stensel, H. D., and Ferguson, J.: Growth kinetics and competition between Methanosarcina and Methanosaeta in mesophilic anaerobic digestion, Water Environment Research, 78, 486–496, https://doi.org/10.2175/106143006X95393, 2006.

De Rosa, M., De Rosa, S., Gambacorta, A., Minale, L., and Bu'lock, J. D.: Chemical structure of the ether lipids of thermophilic acidophilic bacteria of the Caldariella group, Phytochemistry, 16, 1961–1965, https://doi.org/10.1016/0031-9422(77)80105-2, 1977.

Dearing Crampton-Flood, E., Peterse, F., and Sinninghe Damsté, J. S.: Production of branched tetraethers in the marine realm: Svalbard fjord sediments revisited, Organic Geochemistry, 138, 103907, https://doi.org/10.1016/j.orggeochem.2019.103907, 2019.

Díaz-Mendoza, G. A., Krämer, K., von Rönn, G. A., Schwarzer, K., Heinrich, C., Reimers, H.-C., and Winter, C.: Circular structures on the seabed: differentiating between natural and anthropogenic origins—Examples from the Southwestern Baltic Sea, Frontiers in Earth Science, 11, 1170787, 2023.

Ding, S., Kohlhepp, B., Trumbore, S., Küsel, K., Totsche, K.-U., Pohnert, G., Gleixner, G., and Schwab, V. F.: In situ production of core and intact bacterial and archaeal tetraether lipids in groundwater, Organic Geochemistry, 126, 1–12, https://doi.org/10.1016/j.orggeochem.2018.10.005, 2018.

Ehlert von Ahn, C. M., Dellwig, O., Szymczycha, B., Kotwicki, L., Rooze, J., Endler, R., Escher, P., Schmiedinger, I., Sültenfuß, J., Diak, M., Gehre, M., Struck, U., Vogler, S., and Böttcher, M. E.: Submarine groundwater discharge into a semi-enclosed coastal bay of the southern Baltic Sea: A multi-method approach, Oceanologia, 66, 111–138, https://doi.org/10.1016/j.oceano.2024.01.001, 2024.

Elling, F. J., Könneke, M., Nicol, G. W., Stieglmeier, M., Bayer, B., Spieck, E., de la Torre, J. R., Becker, K. W., Thomm, M., Prosser, J. I., Herndl, G. J., Schleper, C., and Hinrichs, K.-U.: Chemotaxonomic characterisation of the thaumarchaeal lipidome, Environmental Microbiology, 19, 2681–2700, https://doi.org/10.1111/1462-2920.13759, 2017.

Engvall, A.-G.: The fate of nitrogen in early diagenesis of Baltic sediments: a study of the sediment-water interface, PhD thesis, University of Stokholm, Stockholm, 16 pp., 1978.

Ettwig, K. F., Zhu, B., Speth, D., Keltjens, J. T., Jetten, M. S. M., and Kartal, B.: Archaea catalyze iron-dependent anaerobic oxidation of methane, Proceedings of the National Academy of Sciences, 113, 12792–12796, https://doi.org/10.1073/pnas.1609534113, 2016.

Fenies, P., Ho, S. L., Hefter, J., and Lee, P.-T.: Impact of anaerobic methanotrophic archaeal input on hydroxylated isoprenoid GDGT-derived temperatures, Organic Geochemistry, 218, 105213, https://doi.org/10.1016/j.orggeochem.2026.105213, 2026.

Galagan, J. E., Nusbaum, C., Roy, A., Endrizzi, M. G., Macdonald, P., FitzHugh, W., Calvo, S., Engels, R., Smirnov, S., Atnoor, D., Brown, A., Allen, N., Naylor, J., Stange-Thomann, N., DeArellano, K., Johnson, R., Linton, L., McEwan, P., McKernan, K., Talamas, J., Tirrell, A., Ye, W., Zimmer, A., Barber, R. D., Cann, I., Graham, D. E., Grahame, D. A., Guss, A. M., Hedderich, R., Ingram-Smith, C., Kuettner, H. C., Krzycki, J. A., Leigh, J. A., Li, W., Liu, J., Mukhopadhyay, B., Reeve, J. N., Smith, K., Springer, T. A., Umayam, L. A., White, O., White, R. H., Conway de Macario, E., Ferry, J. G., Jarrell, K. F., Jing, H., Macario, A. J. L., Paulsen, I., Pritchett, M., Sowers, K. R., Swanson, R. V., Zinder, S. H., Lander, E., Metcalf, W. W., and Birren, B.: The genome of M. acetivorans reveals extensive metabolic and physiological diversity, Genome Research, 12, 532–542, https://doi.org/10.1101/gr.223902, 2002.

Gloor, G. B., Macklaim, J. M., Pawlowsky-Glahn, V., and Egozcue, J. J.: Microbiome datasets are compositional: and this is not optional, Frontiers in Microbiology, 8, 2224, 2017.

González-Toril, E., Gómez, F., Malki, M., and Amils, R.: The isolation and study of Acidophilic microorganisms, in: Methods in Microbiology, vol. 35, Academic Press, 471–510, https://doi.org/10.1016/S0580-9517(08)70023-0, 2006.

Guan, H., Liu, L., Birgel, D., Peckmann, J., Feng, D., and Li, S.: Hydroxylated GDGTs-0 in marine methane seep environments: A putative indicator for archaeal methanogenesis, Organic Geochemistry, 198, 104862, https://doi.org/10.1016/j.orggeochem.2024.104862, 2024.

Haroon, M. F., Hu, S., Shi, Y., Imelfort, M., Keller, J., Hugenholtz, P., Yuan, Z., and Tyson, G. W.: Anaerobic oxidation of methane coupled to nitrate reduction in a novel archaeal lineage, Nature, 500, 567–570, https://doi.org/10.1038/nature12375, 2013.

Hedges, J. I. and Stern, J. H.: Carbon and nitrogen determinations of carbonate-containing solids1, Limnology and Oceanography, 29, 657–663, https://doi.org/10.4319/lo.1984.29.3.0657, 1984.

Hoffmann, J. J. L., Schneider von Deimling, J., Schröder, J. F., Schmidt, M., Held, P., Crutchley, G. J., Scholten, J., and Gorman, A. R.: Complex eyed pockmarks and submarine groundwater discharge revealed by acoustic data and sediment cores in Eckernförde Bay, SW

1406 Baltic Sea, Geochemistry, Geophysics, Geosystems, 21, e2019GC008825,
1407 https://doi.org/10.1029/2019GC008825, 2020.

1408 Hopmans, E. C., Schouten, S., and Sinninghe Damsté, J. S.: The effect of improved
1409 chromatography on GDGT-based palaeoproxies, Organic Geochemistry, 93, 1–6,
1410 https://doi.org/10.1016/j.orggeochem.2015.12.006, 2016.

1411 Hovland, M. and Judd, A. G.: Seabed Pockmarks and Seepages. Impact on Geology, Biology
1412 and the Marine Environment, Graham & Trotman (Kluwer), London, Dordrecht, Boston, 293
1413 pp., 1988.

1414 Hovland, M., Gardner, J. V., and Judd, A. G.: The significance of pockmarks to
1415 understanding fluid flow processes and geohazards, Geofluids, 2, 127–136, 2002.

1416 Huguet, A., Fosse, C., Laggoun-Défarge, F., Toussaint, M.-L., and Derenne, S.: Occurrence
1417 and distribution of glycerol dialkyl glycerol tetraethers in a French peat bog, Organic
1418 Geochemistry, 41, 559–572, https://doi.org/10.1016/j.orggeochem.2010.02.015, 2010.

1419 Huguet, C., Hopmans, E. C., Febo-Ayala, W., Thompson, D. H., Sinninghe Damsté, J. S., and
1420 Schouten, S.: An improved method to determine the absolute abundance of glycerol
1421 dibiphytanyl glycerol tetraether lipids, Organic Geochemistry, 37, 1036–1041,
1422 https://doi.org/10.1016/j.orggeochem.2006.05.008, 2006.

1423 Huguet, C., Fietz, S., and Rosell-Melé, A.: Global distribution patterns of hydroxy glycerol
1424 dialkyl glycerol tetraethers, Organic Geochemistry, 57, 107–118,
1425 https://doi.org/10.1016/j.orggeochem.2013.01.010, 2013.

1426 Iasakov, T. R., Kanapatskiy, T. A., Toshchakov, S. V., Korzhenkov, A. A., Ulyanova, M. O.,
1427 and Pimenov, N. V.: The Baltic Sea methane pockmark microbiome: The new insights into
1428 the patterns of relative abundance and ANME niche separation, Marine Environmental
1429 Research, 173, 105533, https://doi.org/10.1016/j.marenvres.2021.105533, 2022.

1430 Idczak, J., Brodecka-Goluch, A., Łukawska-Matuszewska, K., Graca, B., Gorska, N., Klusek,
1431 Z., Pezacki, P. D., and Bolałek, J.: A geophysical, geochemical and microbiological study of a
1432 newly discovered pockmark with active gas seepage and submarine groundwater discharge
1433 (MET1-BH, central Gulf of Gdańsk, southern Baltic Sea), Science of The Total Environment,
1434 742, 140306, https://doi.org/10.1016/j.scitotenv.2020.140306, 2020.

1435 Inglis, G. N., Farnsworth, A., Lunt, D., Foster, G. L., Hollis, C. J., Pagani, M., Jardine, P. E.,
1436 Pearson, P. N., Markwick, P., Galsworthy, A. M. J., Raynham, L., Taylor, Kyle. W. R., and
1437 Pancost, R. D.: Descent toward the Icehouse: Eocene sea surface cooling inferred from
1438 GDGT distributions, Paleoceanography, 30, 1000–1020,
1439 https://doi.org/10.1002/2014PA002723, 2015.

1440 Ininbergs, K., Bergman, B., Larsson, J., and Ekman, M.: Microbial metagenomics in the
1441 Baltic Sea: Recent advancements and prospects for environmental monitoring, AMBIO, 44,
1442 439–450, https://doi.org/10.1007/s13280-015-0663-7, 2015.

1443 Jakobs, G., Labrenz, M., Rehder, G., Hietanen, S., Kießlich, K., Vogts, A., Blumenberg, M.,
1444 and Schmale, O.: A boreactor approach to investigate the linkage between methane oxidation
1445 and nitrate/nitrite reduction in the pelagic oxic-anoxic transition zone of the Central Baltic
1446 Sea, Frontiers in Marine Science, 3, https://doi.org/10.3389/fmars.2016.00145, 2016.

Jakobsson, M., O'Regan, M., Mörth, C.-M., Stranne, C., Weidner, E., Hansson, J., Gyllencreutz, R., Humborg, C., Elfwing, T., Norkko, A., Norkko, J., Nilsson, B., and Sjöström, A.: Potential links between Baltic Sea submarine terraces and groundwater seeping, Earth Surface Dynamics, 8, 1–15, https://doi.org/10.5194/esurf-8-1-2020, 2020.

Jäntti, H., Ward, B. B., Dippner, J. W., and Hietanen, S.: Nitrification and the ammonia-oxidizing communities in the central Baltic Sea water column, Estuarine, Coastal and Shelf Science, 202, 280–289, https://doi.org/10.1016/j.ecss.2018.01.019, 2018.

Jaśniewicz, D., Klusek, Z., Brodecka-Goluch, A., and Bolałek, J.: Acoustic investigations of shallow gas in the southern Baltic Sea (Polish Exclusive Economic Zone): a review, Geo-Marine Letters, 39, 1–17, https://doi.org/10.1007/s00367-018-0555-5, 2019.

Jaworowski, K., Wagner, R., Modliski, Z., Pokorski, J., Sokołowski, J., and Sokołowski, A.: Marine ecogeology in semi-closed basin: case study on a threat of geogenic pollution of the southern Baltic Sea (Polish Exclusive Economic Zone), Geological Quarterly, 54, 267–288, 2010.

Jensen, J. B., Kuijpers, A., Bennike, O., Laier, T., and Werner, F.: New geological aspects for freshwater seepage and formation in Eckernförde Bay, western Baltic, Continental Shelf Research, 22, 2159–2173, https://doi.org/10.1016/S0278-4343(02)00076-6, 2002.

Jørgensen, B. B., Weber, A., and Zopfi, J.: Sulfate reduction and anaerobic methane oxidation in Black Sea sediments, Deep Sea Research Part I: Oceanographic Research Papers, 48, 2097–2120, https://doi.org/10.1016/S0967-0637(01)00007-3, 2001.

Kaiser, J. and Arz, H. W.: Sources of sedimentary biomarkers and proxies with potential paleoenvironmental significance for the Baltic Sea, Continental Shelf Research, 122, 102–119, https://doi.org/10.1016/j.csr.2016.03.020, 2016.

Kapustina, M., Bubnova, E., and Dudkov, I.: Deep water of the Gdansk Deep (Baltic Sea): variability of hydrology and dissolved oxygen over recent decades, Regional Studies in Marine Science, 93, 104727, https://doi.org/10.1016/j.rsma.2025.104727, 2026.

Kim, B. and Zhang, Y. G.: Methane Index: Towards a quantitative archaeal lipid biomarker proxy for reconstructing marine sedimentary methane fluxes, Geochimica et Cosmochimica Acta, 354, 74–87, https://doi.org/10.1016/j.gca.2023.06.008, 2023.

King, L. H. and MacLean, B.: Pockmarks on the Scotian Shelf, GSA Bulletin, 81, 3141–3148, 1970.

Knittel, K. and Boetius, A.: Anaerobic oxidation of methane: progress with an unknown process, Annual Review of Microbiology, 63, 311–334, https://doi.org/10.1146/annurev.micro.61.080706.093130, 2009.

Koga, Y., Nishihara, M., Morii, H., and Akagawa-Matsushita, M.: Ether polar lipids of methanogenic bacteria: structures, comparative aspects, and biosyntheses, Microbiological Reviews, 57, 164–182, https://doi.org/10.1128/mr.57.1.164-182.1993, 1993.

Kotarba, M. J.: Origin of hydrocarbon gases accumulated in the Middle Cambrian reservoirs of the Polish part of the Baltic region, Geological Quarterly, 54, 197–204, 2010.

Kotarba, M. J. and Lewan, M. D.: Sources of natural gases in Middle Cambrian reservoirs in Polish and Lithuanian Baltic Basin as determined by stable isotopes and hydrous pyrolysis of Lower Palaeozoic source rocks, Chemical Geology, 345, 62–76, https://doi.org/10.1016/j.chemgeo.2013.02.023, 2013.

Kotarba, M. J. and Nagao, K.: Molecular and isotopic compositions and origin of natural gases from Cambrian and Carboniferous-Lower Permian reservoirs of the onshore Polish Baltic region, International Journal of Earth Sciences, 104, 241–261, https://doi.org/10.1007/s00531-014-1063-0, 2015.

Kreuzburg, M., Scholten, J., Hsu, F.-H., Liebetrau, V., Sültenfuß, J., Rapaglia, J., and Schlüter, M.: Submarine groundwater discharge-derived nutrient fluxes in Eckernförde Bay (Western Baltic Sea), Estuaries and Coasts, 46, 1190–1207, https://doi.org/10.1007/s12237-023-01202-0, 2023.

Kuliński, K., Rehder, G., Asmala, E., Bartosova, A., Carstensen, J., Gustafsson, B., Hall, P. O. J., Humborg, C., Jilbert, T., Jürgens, K., Meier, H. E. M., Müller-Karulis, B., Naumann, M., Olesen, J. E., Savchuk, O., Schramm, A., Slomp, C. P., Sofiev, M., Sobek, A., Szymczycha, B., and Undeman, E.: Biogeochemical functioning of the Baltic Sea, Earth System Dynamics, 13, 633–685, https://doi.org/10.5194/esd-13-633-2022, 2022.

Kurowski, S., Łukawska-Matuszewska, K., Čović, A., Jozić, D., and Brodecka-Goluch, A.: Effects of pockmark activity on iron cycling and mineral composition in continental shelf sediments (southern Baltic Sea), Biogeochemistry, 167, 135–154, https://doi.org/10.1007/s10533-024-01127-1, 2024.

Labrenz, M., Sintes, E., Toetzke, F., Zumsteg, A., Herndl, G. J., Seidler, M., and Jürgens, K.: Relevance of a crenarchaeotal subcluster related to Candidatus Nitrosopumilus maritimus to ammonia oxidation in the suboxic zone of the central Baltic Sea, The ISME Journal, 4, 1496–1508, https://doi.org/10.1038/ismej.2010.78, 2010.

Lee, D.-H., Kim, J.-H., Lee, Y. M., Stadnitskaia, A., Jin, Y. K., Niemann, H., Kim, Y.-G., and Shin, K.-H.: Biogeochemical evidence of anaerobic methane oxidation on active submarine mud volcanoes on the continental slope of the Canadian Beaufort Sea, Biogeosciences, 15, 7419–7433, https://doi.org/10.5194/bg-15-7419-2018, 2018.

Lengger, S. K., Kraaij, M., Tjallingii, R., Baas, M., Stuut, J.-B., Hopmans, E. C., Sinninghe Damsté, J. S., and Schouten, S.: Differential degradation of intact polar and core glycerol dialkyl glycerol tetraether lipids upon post-depositional oxidation, Organic Geochemistry, 65, 83–93, https://doi.org/10.1016/j.orggeochem.2013.10.004, 2013.

Leu, A. O., Cai, C., McIlroy, S. J., Southam, G., Orphan, V. J., Yuan, Z., Hu, S., and Tyson, G. W.: Anaerobic methane oxidation coupled to manganese reduction by members of the Methanoperedenaceae, The ISME Journal, 14, 1030–1041, https://doi.org/10.1038/s41396-020-0590-x, 2020.

Li, X., Li, Y., Gao, D., Liu, M., and Hou, L.: Methane production linked to organic matter molecule and methanogenic community in estuarine benthic sediments, Journal of Geophysical Research: Biogeosciences, 127, e2022JG007236, https://doi.org/10.1029/2022JG007236, 2022.

Liu, Q., Charette, M. A., Breier, C. F., Henderson, P. B., McCorkle, D. C., Martin, W., and Dai, M.: Carbonate system biogeochemistry in a subterranean estuary – Waquoit Bay, USA, Geochimica et Cosmochimica Acta, 203, 422–439, https://doi.org/10.1016/j.gca.2017.01.041, 2017.

Liu, X.-L., Summons, R. E., and Hinrichs, K.-U.: Extending the known range of glycerol ether lipids in the environment: structural assignments based on tandem mass spectral fragmentation patterns, Rapid Communications in Mass Spectrometry, 26, 2295–2302, https://doi.org/10.1002/rcm.6355, 2012.

Lu, J., Breitwieser, F. P., Thielen, P., and Salzberg, S. L.: Bracken: estimating species abundance in metagenomics data, PeerJ Computer Science, 3, e104, https://doi.org/10.7717/peerj-cs.104, 2017.

Lu, J., Rincon, N., Wood, D. E., Breitwieser, F. P., Pockrandt, C., Langmead, B., Salzberg, S. L., and Steinegger, M.: Metagenome analysis using the Kraken software suite, Nature Protocols, 17, 2815–2839, https://doi.org/10.1038/s41596-022-00738-y, 2022.

Lü, X., Liu, X.-L., Elling, F. J., Yang, H., Xie, S., Song, J., Li, X., Yuan, H., Li, N., and Hinrichs, K.-U.: Hydroxylated isoprenoid GDGTs in Chinese coastal seas and their potential as a paleotemperature proxy for mid-to-low latitude marginal seas, Organic Geochemistry, 89–90, 31–43, https://doi.org/10.1016/j.orggeochem.2015.10.004, 2015.

Lukawska-Matuszewska, K.: Contribution of non-carbonate inorganic and organic alkalinity to total measured alkalinity in pore waters in marine sediments (Gulf of Gdansk, S-E Baltic Sea), Marine Chemistry, 186, 211–220, https://doi.org/10.1016/j.marchem.2016.10.002, 2016.

Łukawska-Matuszewska, K. and Dwornik, M.: Early diagenesis in anoxic sediments of the Gulf of Gdańsk (southern Baltic Sea): Implications for porewater chemistry and benthic flux of carbonate alkalinity, Frontiers in Earth Science, 13, https://doi.org/10.3389/feart.2025.1593031, 2025.

Łukawska-Matuszewska, K., Brocławik, O., Brodecka-Goluch, A., Rzepa, G., Manecki, M., and Bolałek, J.: Biogeochemical and mineralogical effects of Fe-P-S dynamics in sediments of continental shelf sea: Impact of salinity, oxygen conditions, and catchment area characteristics, Science of The Total Environment, 807, 151035, https://doi.org/10.1016/j.scitotenv.2021.151035, 2022.

Łukawska-Matuszewska, K., Brodecka-Goluch, A., Czachor, A., and Rios-Quintero, R.: Gas bubble release areas as new potential hot spots for water column enrichment with nutrients in eutrophicated sea, Marine Environmental Research, 205, 106981, https://doi.org/10.1016/j.marenvres.2025.106981, 2025.

Lynes, M. M., Jay, Z. J., Kohtz, A. J., and Hatzenpichler, R.: Methylotrophic methanogenesis in the Archaeoglobi revealed by cultivation of Ca. Methanoglobus hypatiae from a Yellowstone hot spring, The ISME Journal, 18, wrae026, https://doi.org/10.1093/ismejo/wrae026, 2024.

Maeder, D. L., Anderson, I., Brettin, T. S., Bruce, D. C., Gilna, P., Han, C. S., Lapidus, A., Metcalf, W. W., Saunders, E., Tapia, R., and Sowers, K. R.: The Methanosarcina barkeri genome: comparative analysis with Methanosarcina acetivorans and Methanosarcina mazei

reveals extensive rearrangement within methanosarcinal genomes, Journal of Bacteriology, 188, 7922–7931, https://doi.org/10.1128/JB.00810-06, 2006.

Majewski, P. and Klusek, Z.: Expressions of shallow gas in the Gdansk Basin, Zeszyty Naukowe Akademii Marynarki Wojennej, 52, 61–71, 2011.

Martens-Habbena, W. and Qin, W.: Archaeal nitrification without oxygen, Science, 375, 27–28, https://doi.org/10.1126/science.abn0373, 2022.

Moore, W. S.: The subterranean estuary: a reaction zone of ground water and sea water, Marine Chemistry, 65, 111–125, https://doi.org/10.1016/S0304-4203(99)00014-6, 1999.

Moore, W. S.: The effect of submarine groundwater discharge on the ocean, Annual Review of Marine Science, 2, 59–88, https://doi.org/10.1146/annurev-marine-120308-081019, 2010.

Niemann, H. and Elvert, M.: Diagnostic lipid biomarker and stable carbon isotope signatures of microbial communities mediating the anaerobic oxidation of methane with sulphate, Organic Geochemistry, 39, 1668–1677, https://doi.org/10.1016/j.orggeochem.2007.11.003, 2008.

O'Reilly, S. S., Jordan, S. F., Monteys, X., Simpson, A. J., Allen, C. C. R., Szpak, M. T., Murphy, B. T., McCarron, S. G., Soong, R., Wu, B., Jenne, A., Grey, A., and Kelleher, B. P.: Production of methane and gaseous compounds by surface microbial activity in a small pockmark field, Dunmanus Bay, Ireland, Estuarine, Coastal and Shelf Science, 255, 107340, https://doi.org/10.1016/j.ecss.2021.107340, 2021.

Palarea-Albaladejo, J. and Martín-Fernández, J. A.: zCompositions — R package for multivariate imputation of left-censored data under a compositional approach, Chemometrics and Intelligent Laboratory Systems, 143, 85–96, https://doi.org/10.1016/j.chemolab.2015.02.019, 2015.

Pancost, R. D., Hopmans, E. C., and Sinninghe Damsté, J. S.: Archaeal lipids in Mediterranean cold seeps: molecular proxies for anaerobic methane oxidation, Geochimica et Cosmochimica Acta, 65, 1611–1627, https://doi.org/10.1016/S0016-7037(00)00562-7, 2001.

Parsons, T. R., Maita, Y., and Lalli, C. M.: A Manual of Chemical & Biological Methods for Seawater Analysis, Pergamon Press, 188 pp., 1984.

Peterse, F., Kim, J.-H., Schouten, S., Kristensen, D. K., Koç, N., and Sinninghe Damsté, J. S.: Constraints on the application of the MBT/CBT palaeothermometer at high latitude environments (Svalbard, Norway), Organic Geochemistry, 40, 692–699, https://doi.org/10.1016/j.orggeochem.2009.03.004, 2009.

Petrick, B., Reuning, L., and Martínez-García, A.: Distribution of glycerol dialkyl glycerol tetraethers (GDGTs) in microbial mats from Holocene and Miocene sabkha sediments, Frontiers in Earth Science, 7, https://doi.org/10.3389/feart.2019.00310, 2019.

Piekarek-Jankowska, H.: Hydrochemical effects of submarine groundwater discharge to the Puck Bay [Southern Baltic Sea, Poland], Geographia Polonica, 67, 103–119, 1996.

Pimenov, N. V., Ulyanova, M. O., Kanapatsky, T. A., Veslopolova, E. F., Sigalevich, P. A., and Sivkov, V. V.: Microbially mediated methane and sulfur cycling in pockmark sediments

of the Gdansk Basin, Baltic Sea, Geo-Marine Letters, 30, 439–448, https://doi.org/10.1007/s00367-010-0200-4, 2010.

Pokorski, J.: Geological section through the lower Paleozoic strata of the Polish part of the Baltic region, Geological Quarterly, 54, 123–130, 2010.

Purkamo, L., von Ahn, C. M. E., Jilbert, T., Muniruzzaman, M., Bange, H. W., Jenner, A.-K., Böttcher, M. E., and Virtasalo, J. J.: Impact of submarine groundwater discharge on biogeochemistry and microbial communities in pockmarks, Geochimica et Cosmochimica Acta, 334, 14–44, https://doi.org/10.1016/j.gca.2022.06.040, 2022.

Quast, C., Pruesse, E., Yilmaz, P., Gerken, J., Schweer, T., Yarza, P., Peplies, J., and Glöckner, F. O.: The SILVA ribosomal RNA gene database project: improved data processing and web-based tools, Nucleic Acids Research, 41, D590–D596, https://doi.org/10.1093/nar/gks1219, 2013.

Quinn, T. P., Erb, I., Gloor, G., Notredame, C., Richardson, M. F., and Crowley, T. M.: A field guide for the compositional analysis of any-omics data, GigaScience, 8, giz107, https://doi.org/10.1093/gigascience/giz107, 2019.

R Core Team: R: A language and environment for statistical computing. R Foundation for Statistical Computing, 2023.

Reeburgh, W. S.: Oceanic methane biogeochemistry, Chemical Reviews, 107, 486–513, https://doi.org/10.1021/cr050362v, 2007.

Rinke, C., Chuvochina, M., Mussig, A. J., Chaumeil, P.-A., Davín, A. A., Waite, D. W., Whitman, W. B., Parks, D. H., and Hugenholtz, P.: A standardized archaeal taxonomy for the Genome Taxonomy Database, Nature Microbiology, 6, 946–959, https://doi.org/10.1038/s41564-021-00918-8, 2021.

Rogers, D. R. and Casciotti, K. L.: Abundance and diversity of archaeal ammonia oxidizers in a coastal groundwater system, Applied and Environmental Microbiology, 76, 7938–7948, https://doi.org/10.1128/AEM.02056-09, 2010.

Rossel, P. E., Lipp, J. S., Fredricks, H. F., Arnds, J., Boetius, A., Elvert, M., and Hinrichs, K.-U.: Intact polar lipids of anaerobic methanotrophic archaea and associated bacteria, Organic Geochemistry, 39, 992–999, https://doi.org/10.1016/j.orggeochem.2008.02.021, 2008.

Ruiz-González, C., Rodellas, V., and Garcia-Orellana, J.: The microbial dimension of submarine groundwater discharge: current challenges and future directions, FEMS Microbiology Reviews, 45, fuab010, https://doi.org/10.1093/femsre/fuab010, 2021.

Santoro, A. E., Francis, C. A., De Sieyes, N. R., and Boehm, A. B.: Shifts in the relative abundance of ammonia-oxidizing bacteria and archaea across physicochemical gradients in a subterranean estuary, Environmental Microbiology, 10, 1068–1079, https://doi.org/10.1111/j.1462-2920.2007.01547.x, 2008.

Schlüter, M., Sauter, E. J., Andersen, C. E., Dahlgaard, H., and Dando, P. R.: Spatial distribution and budget for submarine groundwater discharge in Eckernförde Bay (Western Baltic Sea), Limnology and Oceanography, 49, 157–167, https://doi.org/10.4319/lo.2004.49.1.0157, 2004.

Schmuck, E. A. and Paull, C. K.: Evidence for gas accumulation associated with diapirism and gas hydrates at the head of the Cape Fear Slide, Geo-Marine Letters, 13, 145–152, https://doi.org/10.1007/BF01593187, 1993.

Schouten, S., Hopmans, E. C., Schefuß, E., and Sinninghe Damsté, J. S.: Distributional variations in marine crenarchaeotal membrane lipids: a new tool for reconstructing ancient sea water temperatures?, Earth and Planetary Science Letters, 204, 265–274, https://doi.org/10.1016/S0012-821X(02)00979-2, 2002.

Schouten, S., Hopmans, E. C., and Sinninghe Damsté, J. S.: The organic geochemistry of glycerol dialkyl glycerol tetraether lipids: A review, Organic Geochemistry, 54, 19–61, https://doi.org/10.1016/j.orggeochem.2012.09.006, 2013.

Shaw, J., Courtney, R. C., and Currie, J. R.: Marine geology of St. George's Bay, Newfoundland, as interpreted from multibeam bathymetry and back-scatter data, Geo-Marine Letters, 17, 188–194, https://doi.org/10.1007/s003670050025, 1997.

Sinninghe Damsté, J. S.: Spatial heterogeneity of sources of branched tetraethers in shelf systems: The geochemistry of tetraethers in the Berau River delta (Kalimantan, Indonesia), Geochimica et Cosmochimica Acta, 186, 13–31, https://doi.org/10.1016/j.gca.2016.04.033, 2016.

Sinninghe Damsté, J. S., Schouten, S., Hopmans, E. C., Duin, A. C. T. van, and Geenevasen, J. A. J.: Crenarchaeol, Journal of Lipid Research, 43, 1641–1651, https://doi.org/10.1194/jlr.M200148-JLR200, 2002.

Sinninghe Damsté, J. S., Warden, L. A., Berg, C., Jürgens, K., and Moros, M.: Evaluation of the distributions of hydroxylated glycerol dibiphytanyl glycerol tetraethers (GDGTs) in Holocene Baltic Sea sediments for reconstruction of sea surface temperature: the effect of changing salinity, Climate of the Past, 18, 2271–2288, https://doi.org/10.5194/cp-18-2271-2022, 2022.

Słowakiewicz, M., Whitaker, F., Thomas, L., Tucker, M. E., Zheng, Y., Gedl, P., and Pancost, R. D.: Biogeochemistry of intertidal microbial mats from Qatar: New insights from organic matter characterisation, Organic Geochemistry, 102, 14–29, https://doi.org/10.1016/j.orggeochem.2016.09.006, 2016.

Sowers, K. R., Boone, J. E., and Gunsalus, R. P.: Disaggregation of Methanosarcina spp. and growth as single cells at elevated osmolarity, Applied and Environmental Microbiology, 59, 3832–3839, https://doi.org/10.1128/aem.59.11.3832-3839.1993, 1993.

Stadnitskaia, A., Muyzer, G., Abbas, B., Coolen, M. J. L., Hopmans, E. C., Baas, M., van Weering, T. C. E., Ivanov, M. K., Poludetkina, E., and Sinninghe Damsté, J. S.: Biomarker and 16S rDNA evidence for anaerobic oxidation of methane and related carbonate precipitation in deep-sea mud volcanoes of the Sorokin Trough, Black Sea, Marine Geology, 217, 67–96, https://doi.org/10.1016/j.margeo.2005.02.023, 2005.

Stegen, J. C., Fredrickson, J. K., Wilkins, M. J., Konopka, A. E., Nelson, W. C., Arntzen, E. V., Chrisler, W. B., Chu, R. K., Danczak, R. E., Fansler, S. J., Kennedy, D. W., Resch, C. T., and Tfaily, M.: Groundwater–surface water mixing shifts ecological assembly processes and stimulates organic carbon turnover, Nature Communications, 7, 11237, https://doi.org/10.1038/ncomms11237, 2016.

Szczepańska, T. and Uścinowicz, S.: Atlas geochemiczny południowego Bałtyku, Państwowy Instytut Geologiczny, Warszawa, 1–55 pp., 1994.

Szymczak-Żyła, M. and Lubecki, L.: Biogenic and anthropogenic sources of sedimentary organic matter in marine coastal areas: A multi-proxy approach based on bulk and molecular markers, Marine Chemistry, 239, 104069, https://doi.org/10.1016/j.marchem.2021.104069, 2022.

Szymczycha, B., Kroeger, K. D., and Pempkowiak, J.: Significance of groundwater discharge along the coast of Poland as a source of dissolved metals to the southern Baltic Sea, Marine Pollution Bulletin, 109, 151–162, https://doi.org/10.1016/j.marpolbul.2016.06.008, 2016.

Szymczycha, B., Kłostowska, Ż., Kuliński, K., Winogradow, A., Jakacki, J., Klusek, Z., Grabowski, M., Brodecka-Goluch, A., Graca, B., Stokowski, M., Koziorowska, K., and Rak, D.: Deep submarine groundwater discharge indicated by pore water chloride anomalies in the Gulf of Gdańsk, southern Baltic Sea, E3S Web of Conferences, 54, 00035, https://doi.org/10.1051/e3sconf/20185400035, 2018.

Taniguchi, M., Dulai, H., Burnett, K. M., Santos, I. R., Sugimoto, R., Stieglitz, T., Kim, G., Moosdorf, N., and Burnett, W. C.: Submarine groundwater discharge: updates on its measurement techniques, geophysical drivers, magnitudes, and effects, Frontiers in Environmental Science, 7, https://doi.org/10.3389/fenvs.2019.00141, 2019.

Taylor, M. H., Dillon, W. P., and Pecher, I. A.: Trapping and migration of methane associated with the gas hydrate stability zone at the Blake Ridge Diapir: new insights from seismic data, Marine Geology, 164, 79–89, https://doi.org/10.1016/S0025-3227(99)00128-0, 2000.

Treude, T., Niggemann, J., Kallmeyer, J., Wintersteller, P., Schubert, C. J., Boetius, A., and Jørgensen, B. B.: Anaerobic oxidation of methane and sulfate reduction along the Chilean continental margin, Geochimica et Cosmochimica Acta, 69, 2767–2779, https://doi.org/10.1016/j.gca.2005.01.002, 2005.

Uścinowicz, S. (Ed.): Geochemistry of Baltic Sea surface sediments, Polish Geological Institute–National Research Institute, Warsaw, 356 pp., 2011.

Vaksmaa, A., Guerrero-Cruz, S., van Alen, T. A., Cremers, G., Ettwig, K. F., Lüke, C., and Jetten, M. S. M.: Enrichment of anaerobic nitrate-dependent methanotrophic 'Candidatus Methanoperedens nitroreducens' archaea from an Italian paddy field soil, Appl Microbiol Biotechnol, 101, 7075–7084, https://doi.org/10.1007/s00253-017-8416-0, 2017.

Varma, D., Hopmans, E. C., van Kemenade, Z. R., Kusch, S., Berg, S., Bale, N. J., Sangiorgi, F., Reichart, G.-J., Sinninghe Damsté, J. S., and Schouten, S.: Evaluating isoprenoidal hydroxylated GDGT-based temperature proxies in surface sediments from the global ocean, Geochimica et Cosmochimica Acta, 370, 113–127, https://doi.org/10.1016/j.gca.2023.12.019, 2024.

Virtasalo, J. J., Schröder, J. F., Luoma, S., Majaniemi, J., Mursu, J., and Scholten, J.: Submarine groundwater discharge site in the First Salpausselkä ice-marginal formation, south Finland, Solid Earth, 10, 405–423, https://doi.org/10.5194/se-10-405-2019, 2019.

Wakeham, S. G., Lewis, C. M., Hopmans, E. C., Schouten, S., and Sinninghe Damsté, J. S.: Archaea mediate anaerobic oxidation of methane in deep euxinic waters of the Black Sea,

Geochimica et Cosmochimica Acta, 67, 1359–1374, https://doi.org/10.1016/S0016-7037(02)01220-6, 2003.

Waters, E., Hohn, M. J., Ahel, I., Graham, D. E., Adams, M. D., Barnstead, M., Beeson, K. Y., Bibbs, L., Bolanos, R., Keller, M., Kretz, K., Lin, X., Mathur, E., Ni, J., Podar, M., Richardson, T., Sutton, G. G., Simon, M., Söll, D., Stetter, K. O., Short, J. M., and Noordewier, M.: The genome of Nanoarchaeum equitans: Insights into early archaeal evolution and derived parasitism, Proceedings of the National Academy of Sciences, 100, 12984–12988, https://doi.org/10.1073/pnas.1735403100, 2003.

Weijers, J. W. H., Schouten, S., Hopmans, E. C., Geenevasen, J. A. J., David, O. R. P., Coleman, J. M., Pancost, R. D., and Sinninghe Damsté, J. S.: Membrane lipids of mesophilic anaerobic bacteria thriving in peats have typical archaeal traits, Environmental Microbiology, 8, 648–657, https://doi.org/10.1111/j.1462-2920.2005.00941.x, 2006.

Weijers, J. W. H., Lim, K. L. H., Aquilina, A., Sinninghe Damsté, J. S., and Pancost, R. D.: Biogeochemical controls on glycerol dialkyl glycerol tetraether lipid distributions in sediments characterized by diffusive methane flux, Geochemistry, Geophysics, Geosystems, 12, 1–15, https://doi.org/10.1029/2011GC003724, 2011.

Welte, C., Kröninger, L., and Deppenmeier, U.: Experimental evidence of an acetate transporter protein and characterization of acetate activation in aceticlastic methanogenesis of Methanosarcina mazei, FEMS Microbiology Letters, 359, 147–153, https://doi.org/10.1111/1574-6968.12550, 2014.

Werner, F.: Depressions in mud sediments (Eckernfoerde Bay, Baltic Sea), related to sub-bottom and currents, Meyniana, 30, 99–104, 1978.

Wever, Th. F., Abegg, F., Fiedler, H. M., Fechner, G., and Stender, I. H.: Shallow gas in the muddy sediments of Eckernförde Bay, Germany, Continental Shelf Research, 18, 1715–1739, https://doi.org/10.1016/S0278-4343(98)00055-7, 1998.

Whiticar, M. J.: Diagenetic relationships of methanogenesis, nutrients, acoustic turbidity, pockmarks and freshwater seepages in Eckernförde Bay, Marine Geology, 182, 29–53, https://doi.org/10.1016/S0025-3227(01)00227-4, 2002.

Whiticar, M. J. and Werner, F.: Pockmarks: Submarine vents of natural gas or freshwater seeps?, Geo-Marine Letters, 1, 193–199, https://doi.org/10.1007/BF02462433, 1981.

Wickham, H.: ggplot2: Elegant Graphics for Data Analysis, Springer International Publishing, 260 pp., 2016.

Wilson, S. J., Song, B., Anderson, I. C., and Tobias, C. R.: Nitrification in a subterranean estuary: An ex situ and in situ method comparison determines nitrate is available for discharge, Journal of Geophysical Research: Biogeosciences, 129, e2023JG007876, https://doi.org/10.1029/2023JG007876, 2024.

Wittenborn, A. K., Bauersachs, T., Hassenrück, C., Käding, K., Wäge-Recchioni, J., Jürgens, K., Arz, H. W., and Kaiser, J.: Nitrosopumilus as main source of isoprenoid glycerol dialkyl glycerol tetraether lipids in the central Baltic Sea, Frontiers in Microbiology, 14, https://doi.org/10.3389/fmicb.2023.1216130, 2023.

Wood, D. E., Lu, J., and Langmead, B.: Improved metagenomic analysis with Kraken 2, Genome Biology, 20, 257, https://doi.org/10.1186/s13059-019-1891-0, 2019.

Yi, X., Brandt, K. K., Xue, S., Peng, J., Wang, Y., Li, M., Deng, Y., and Duan, G.: Niche differentiation and biogeography of Bathyarchaeia in paddy soil ecosystems: a case study in eastern China, Environmental Microbiome, 19, 13, https://doi.org/10.1186/s40793-024-00555-8, 2024.

Yu, T., Fu, L., Wang, Y., Dong, Y., Chen, Y., Wegener, G., Cheng, L., and Wang, F.: Thermophilic Hadarchaeota grow on long-chain alkanes in syntrophy with methanogens, Nature Communications, 15, 6560, https://doi.org/10.1038/s41467-024-50883-z, 2024.

Zehnder, A. J. B. and Brock, T. D.: Anaerobic methane oxidation: occurrence and ecology, Applied and Environmental Microbiology, 39, 194–204, https://doi.org/10.1128/aem.39.1.194-204.1980, 1980.

Zell, C., Kim, J.-H., Hollander, D., Lorenzoni, L., Baker, P., Silva, C. G., Nittrouer, C., and Sinninghe Damsté, J. S.: Sources and distributions of branched and isoprenoid tetraether lipids on the Amazon shelf and fan: Implications for the use of GDGT-based proxies in marine sediments, Geochimica et Cosmochimica Acta, 139, 293–312, https://doi.org/10.1016/j.gca.2014.04.038, 2014.

Zeng, Z., Chen, H., Yang, H., Chen, Y., Yang, W., Feng, X., Pei, H., and Welander, P. V.: Identification of a protein responsible for the synthesis of archaeal membrane-spanning GDGT lipids, Nature Communications, 13, 1545, https://doi.org/10.1038/s41467-022-29264-x, 2022.

Zhang, Y. G., Zhang, C. L., Liu, X.-L., Li, L., Hinrichs, K.-U., and Noakes, J. E.: Methane Index: A tetraether archaeal lipid biomarker indicator for detecting the instability of marine gas hydrates, Earth and Planetary Science Letters, 307, 525–534, https://doi.org/10.1016/j.epsl.2011.05.031, 2011.

Zhang, Z., Shan, H., Feng, X., Jia, Z., Jiang, L., Wang, S., and Zhu, C.: Review of research progress on the impact of submarine groundwater discharge on pockmark formation and evolution, Journal of Marine Science and Engineering, 13, 1070, https://doi.org/10.3390/jmse13061070, 2025.

Zhou, Z., Pan, J., Wang, F., Gu, J.-D., and Li, M.: Bathyarchaeota: globally distributed metabolic generalists in anoxic environments, FEMS Microbiology Reviews, 42, 639–655, https://doi.org/10.1093/femsre/fuy023, 2018.

Zinke, L. A., Glombitza, C., Bird, J. T., Røy, H., Jørgensen, B. B., Lloyd, K. G., Amend, J. P., and Reese, B. K.: Microbial organic matter degradation potential in Baltic Sea sediments is influenced by depositional conditions and in situ geochemistry, Applied and Environmental Microbiology, 85, e02164-18, https://doi.org/10.1128/AEM.02164-18, 2019.